AD-A080 804 HARRY DIAMOND LABS ADELPHI MD F/G 20/14
MODIFICATION OF THE AURORA ELECTROMAGNETIC ENVIRONMENT: EXPERIM--ETC(U)
OCT 79 R P MANRIQUEZ, G MERKEL, D J SPOHN
UNCLASSIFIED HDL-PR-79-5 NL

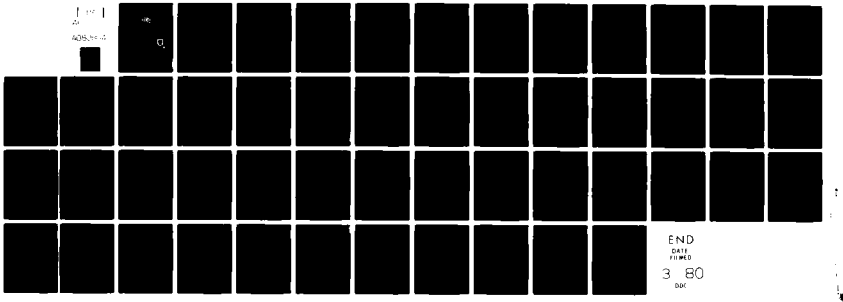

END
DATE FILMED
3 80
DDC

HDL-PR-79-5

October 1979

Modification of the AURORA Electromagnetic Environment: Experiment and Interpretation

Progress Rept.

by Rolando P. Manriquez
George Merkel
Daniel J. Spohn

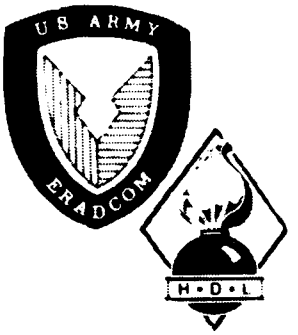

U.S. Army Electronics Research
and Development Command
Harry Diamond Laboratories
Adelphi, MD 20783

This work was sponsored by the Defense Nuclear Agency under
Subtask R99QAXEB088, Work Unit 81, EMP Service RGN.

Approved for public release; distribution unlimited.

The findings in this report are not to be construed as an official Department of the Army position unless so designated by other authorized documents.

Citation of manufacturers' or trade names does not constitute an official indorsement or approval of the use thereof.

Destroy this report when it is no longer needed. Do not return it to the originator.

UNCLASSIFIED

SECURITY CLASSIFICATION OF THIS PAGE (When Data Entered)

REPORT DOCUMENTATION PAGE		READ INSTRUCTIONS BEFORE COMPLETING FORM
1. REPORT NUMBER HDL-PR-79-5	2. GOVT ACCESSION NO.	3. RECIPIENT'S CATALOG NUMBER
4. TITLE (and Subtitle) Modification of the AURORA Electromagnetic Environment: Experiment and Interpretation		5. TYPE OF REPORT & PERIOD COVERED Progress Report 6. PERFORMING ORG. REPORT NUMBER
7. AUTHOR(s) Rolando P. Manriquez George Merkel Daniel J. Spohn		8. CONTRACT OR GRANT NUMBER(s)
9. PERFORMING ORGANIZATION NAME AND ADDRESS Harry Diamond Laboratories 2800 Powder Mill Road Adelphi, MD 20783		10. PROGRAM ELEMENT, PROJECT, TASK AREA & WORK UNIT NUMBERS Program Ele: 6.27.04.H
11. CONTROLLING OFFICE NAME AND ADDRESS Defense Nuclear Agency Washington, DC 20305		12. REPORT DATE October 1979 13. NUMBER OF PAGES 50
14. MONITORING AGENCY NAME & ADDRESS(if different from Controlling Office)		15. SECURITY CLASS. (of this report) UNCLASSIFIED 15a. DECLASSIFICATION/DOWNGRADING SCHEDULE

16. DISTRIBUTION STATEMENT (of this Report)

Approved for public release; distribution unlimited.

17. DISTRIBUTION STATEMENT (of the abstract entered in Block 20, if different from Report)

18. SUPPLEMENTARY NOTES

This work was sponsored by the Defense Nuclear Agency under Subtask R99QAXEB088, Work Unit 81, EMP Service RGN.
DRCMS Code: 36AA.6000.62704
HDL Project: E058E3

19. KEY WORDS (Continue on reverse side if necessary and identify by block number)

Transmission line
Ionizing radiation
Collision dominated plasma
Nuclear electromagnetic pulse
Lumped parameter model

20. ABSTRACT (Continue on reverse side if necessary and identify by block number)

In a series of experiments, we determined that a simple parallel plate transmission line would behave in a predictable manner when subjected to the 13-MeV-thick target bremsstrahlung produced by the AURORA flash x-ray machine. During the experiment, the following parameters were measured: current into the transmission line, current through the matched termination of the transmission line, the electric field at the bottom plate along the

DD FORM 1 JAN 73 1473 EDITION OF 1 NOV 65 IS OBSOLETE

UNCLASSIFIED

SECURITY CLASSIFICATION OF THIS PAGE (When Data Entered)

20. Abstract (Cont'd)

center of the transmission line, and a component of the magnetic field at the center of the transmission line. The experimental results were interpreted with a simple lumped parameter model of the transmission line.

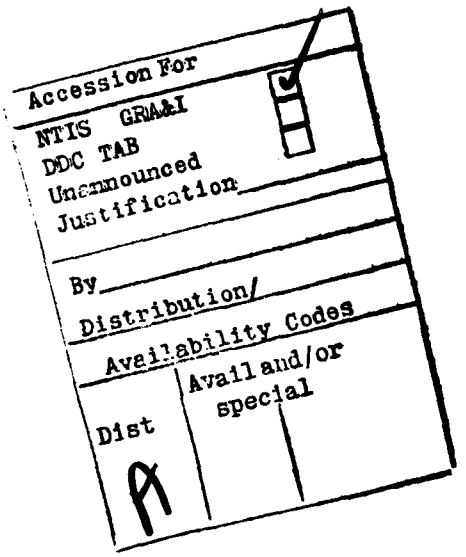

CONTENTS

FIGURES

FIGURES (Cont'd)

FIGURES (Cont'd)

TABLE

1. INTRODUCTION

Our major goal in the work reported here was to ascertain whether the electromagnetic field produced by the AURORA thick target bremsstrahlung could be modified in a predictable fashion by using a parallel plate transmission line. If this prediction can be shown, then possibly it might be feasible to suggest this as a method of tailoring the combined electromagnetic and ionizing radiation so that it more closely resembles the characteristics of the radiation environment predicted for a tactical nuclear weapon. This work was not an attempt to design a tactical electromagnetic pulse (EMP) simulator, but rather was directed toward gaining insight and developing tools that would be of value in designing a larger test facility, one that could be used to verify EMP source-region coupling calculations and possibly even test some actual tactical systems. The experimental measurements reported in this paper were carried out in the fall of 1977.

2. REQUIREMENT FOR MODIFICATION

The AURORA Flash X-Ray Facility at the Harry Diamond Laboratories was designed basically to study high intensity transient (nuclear) radiation effects on electronics TREE). It produces high intensity ionizing radiation over a relatively small volume. The resulting isodose contours produced by the 13-MeV-thick target bremsstrahlung in the metallically shielded AURORA test cell are shown in figure 1.

The components necessary to simulate tactical nuclear EMP are a time varying electric (E-) field, a time varying magnetic (H-) field, a time varying Compton electric current, and time varying air conductivity. Therefore, at first look, the AURORA test cell, which incorporates all these components, might seem to be an ideal candidate for the simulation of a tactical nuclear EMP. But comparisons of measured field data* and the accepted Defense Nuclear Agency threat criteria indicate serious differences in temporal behavior and direction and magnitude of the various components.

We can gain more insight into the problems that arise by considering the possibility of using the *unmodified* AURORA as a tactical nuclear EMP simulator. Let us simplify matters by considering the wave equations for a spatially and temporally homogeneous conducting isotropic medium. The situation inside the AURORA test cell is actually not homogeneous, and the medium, the ionized air, is time varying. However, the consideration of all the variables would require the use of such a complicated computer code that essential physics would tend to be obscured, and insight into the actual simulation problem would be lost.

**Electric field data discussed later in this section and unpublished magnetic field data were taken by Denis Whittaker of the AURORA staff.*

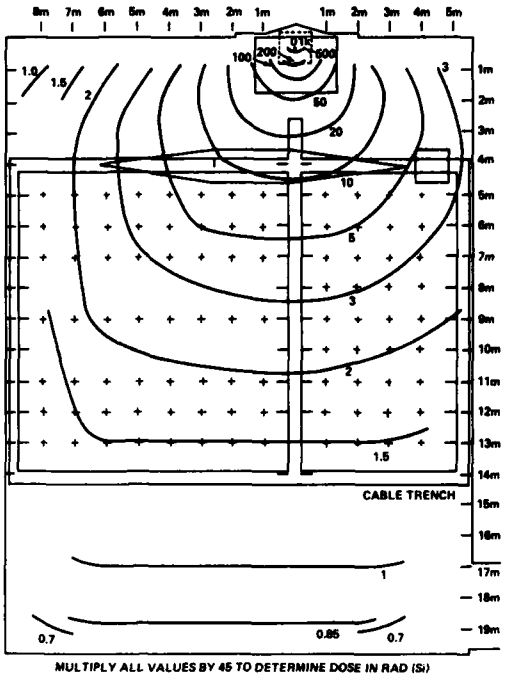

Figure 1. AURORA isodose contours and transmission line in test cell.

Let us consider the wave equations inside the AURORA test cell.

For the E-field, we have

$$\nabla^2 E - \mu_0 \left(\sigma \frac{\partial E}{\partial t} + \varepsilon_0 \frac{\partial^2 E}{\partial t^2} \right) = \mu_0 \frac{\partial J_c}{\partial t} + \frac{\nabla \rho}{\varepsilon_0} \quad , \tag{1}$$

where σ is the air conductivity, J_c is the Compton current, and ρ is the charge density in the test cell ionized air. For the H-field, we have

$$\nabla^2 H - \mu_0 \left(\sigma \frac{\partial H}{\partial t} + \varepsilon_0 \frac{\partial^2 H}{\partial t^2} \right) = -\nabla \times J_c \quad . \tag{2}$$

If we had no Compton current and resulting air conductivity, the situation would be greatly simplified because the above two complicated

wave equations would become the two relatively simple free space wave equations

$$\nabla^2 E - \mu_0 \varepsilon_0 \frac{\partial^2 E}{\partial t^2} = 0 \qquad (3a)$$

and

$$\nabla^2 H - \mu_0 \varepsilon_0 \frac{\partial^2 H}{\partial t^2} = 0 \qquad (3b)$$

and our simulation problem would be similar to the exoatmospheric EMP simulation.

Now consider another extreme: suppose the conducting current were much greater than the displacement current. Then

$$\sigma E >> \varepsilon_0 \frac{\partial E}{\partial t} \quad , \qquad (4)$$

or in the frequency domain

$$\sigma E(\omega) >> \varepsilon_0 \omega E(\omega) \quad . \qquad (5)$$

The original wave equations (1) and (2) now become diffusion equations,

$$\nabla^2 E - \mu_0 \sigma \frac{\partial E}{\partial t} = \mu_0 \frac{\partial J_c}{\partial t} + \frac{\nabla \rho}{\varepsilon_0} \qquad (6)$$

and

$$\nabla^2 H - \mu_0 \sigma \frac{\partial H}{\partial t} = -\nabla \times J_c \qquad (7)$$

Let us assume that the Compton current variation is relatively slow and that the charge gradient is small. Then

$$\nabla^2 E - \mu_0 \sigma \frac{\partial E}{\partial t} = 0 \quad , \tag{8}$$

or in the time domain

$$\nabla^2 E = j\omega\mu_0\sigma E \quad . \tag{9}$$

Let E_z be the E component along the AURORA test cell wall and x the distance away from the wall. Then

$$\frac{d^2 E_z}{dx^2} = j\omega\mu_0\sigma E_z \tag{10}$$

$$= \tau^2 E_z \quad ,$$

where

$$\tau^2 = j\omega\mu_0\sigma \quad ,$$

and

$$\tau = (1 + j)\sqrt{2\pi f \mu_0 \sigma}$$

$$= (1 + j)/\delta \quad ,$$

where

$$\delta = \frac{1}{\sqrt{2\pi f \mu_0 \sigma}} \tag{11}$$

and

$$E_z = C_1 e^{-\tau x} + C_2 e^{\tau x} \quad .$$

The AURORA test cell wall is a "perfect" conductor; therefore, $E_z = 0$ along the test cell wall, $x = 0$, and we have

$$0 = C_1 + C_2$$

or

$$C_1 = -C_2 = (\text{constant}) \quad .$$

Finally,

$$E_z = (\text{constant}) \left(e^{-x/\delta} e^{-jx/\delta} - e^{+x/\delta} e^{+jx/\delta} \right) \quad . \tag{12}$$

Equation (12), which applies when $\sigma E >> \varepsilon_0 (dE/dt)$, is an expression that can be employed to estimate the region (distance), δ, away from the conducting AURORA test cell walls in which the skin effect (in the conducting air) short-circuits the E-field parallel to the AURORA test cell walls.

Assume that $\sigma = 10^{-3}$ mho/m; then

$$\delta = \frac{1}{\sqrt{2\pi f 4\pi 10^{-7} 10^{-3}}} \tag{13}$$

$$= \frac{1.125 \left(10^4\right)}{\sqrt{f}} \quad .$$

For $f = 10^8$ Hz, $\delta = 1.1$ m; for $f = 10^9$ Hz, $\delta = 0.36$ m.

A rough estimate of the horizontal E-field in the center of the AURORA test cell when $\sigma E >> \varepsilon_0(\partial E/\partial t)$ can be obtained by assuming that the E-field builds up until conduction current cancels Compton current; that is,

$$\sigma E = -J_c \quad . \tag{14}$$

Actually, there would probably be some vertical field near the AURORA test cell floor, ceiling, and walls because the Compton current from the AURORA hot spot does not just go to the back of the AURORA test cell, but spreads out, and a portion of the Compton current returns to the hot spot via the side walls, the ceiling, and the floor. This return is illustrated in figure 2.

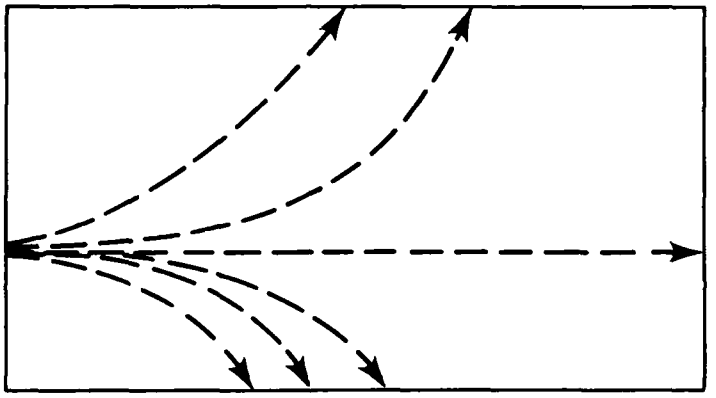

Figure 2. Sketch of average Compton current trajectories.

3. MEASUREMENT OF AURORA VERTICAL ELECTRIC FIELD

When the AURORA fires, some of the Compton electrons produced by the thick target bremsstrahlung impinge on the floor and generate a vertical E-field. To orient ourselves, we need to know the magnitude of the vertical E-field on the test cell floor even though it may not be the major component of the field produced by the AURORA Compton electron drivers.

The values of the vertical E-field and vertical dE/dt along the AURORA test cell floor, 5 m from the front test cell wall, were measured with an EG&G PMD-1 E-field sensor and with a parallel grid sensor

suggested by Victor van Lint (Mission Research Corp.). The grid sensor was connected to an emitter follower with a high impedance input so that the air conductivity did not influence the accuracy of the E-field measurement. Even though the EG&G sensor was designed to be used in a vacuum, its values agreed to within 20 percent of those obtained with the van Lint sensor. The measurements were restricted to the test cell floor because, if the sensor were positioned off the ground plane, the cables to the sensors would perturb the field that the sensor was supposed to measure. With the sensors on the test cell floor, the coaxial cables and the emitter follower could be buried under the test cell so that they did not perturb the fields in the test cell. Figure 1 shows the AURORA isodose contours and the position of our first generation vertical E-field enhancing transmission line.

A typical vertical E-field measurement at a distance of 5 m from the front of the test cell is shown in figure 3. We need to increase this field if we want our simulator to produce a vertical field greater than 7 kV. This field is the purpose of the transmission line. The magnitude of the vertical E-field is probably a maximum on the AURORA test cell floor. If the vertical E-field were measured off the floor, intuition and symmetry arguments tell us that the field would decrease in magnitude and then change direction as the ceiling were approached. Van Lint is designing an E-field sensor that should be able to measure the E-field at all points in the AURORA test cell.

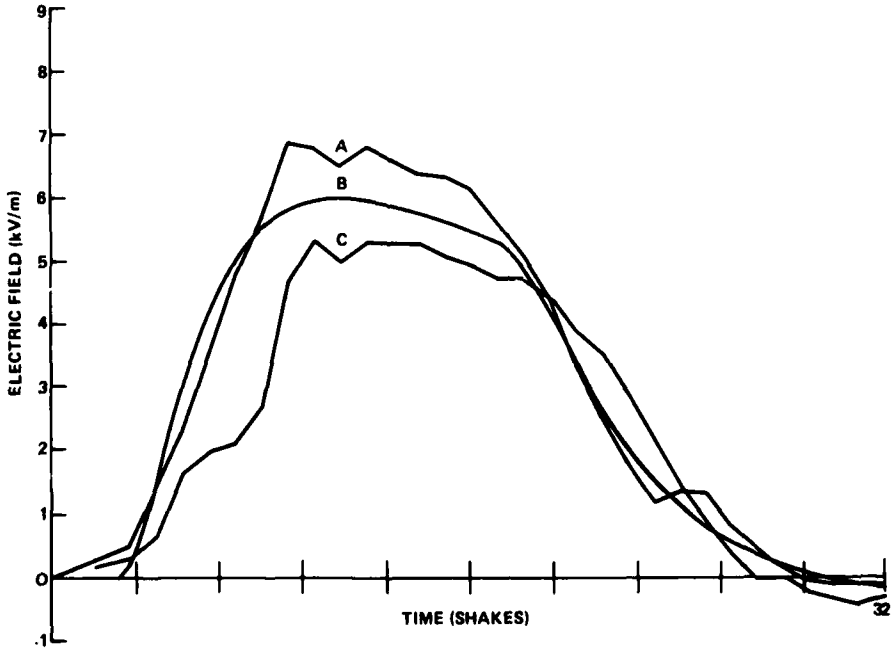

Figure 3. Typical vertical electric-field measurements with Air Force Weapons Laboraotry sensor: (A) AURORA shot 2352, (B) fit with equation (25), and (C) AURORA shot 2351.

4. TRANSMISSION LINE SIMULATOR

The use of a parallel plate transmission line with the ionizing radiation of the AURORA to simulate the electromagnetic environment that is associated with a tactical nuclear device appears to be a basic approach that is also natural. Consider the transmission line equations and Maxwell's equations:

Transmission line equations	Field equations
$\frac{\partial v}{\partial x} = -\left(R + L\frac{\partial}{\partial t}\right) i$,	$\nabla \times E = -\mu_0 \frac{\partial H}{\partial t}$,
$\frac{\partial i}{\partial x} = -\left(G + C\frac{\partial}{\partial t}\right) v$,	$\nabla \times H = \left(\sigma + \varepsilon_0 \frac{\partial}{\partial t}\right) E$.

But R, the resistance of the transmission line plate, is insignificant:

$$\frac{\partial v}{\partial x} = -L\frac{\partial}{\partial t} i \quad ,$$

$$\frac{\partial i}{\partial x} = -\left(G + C\frac{\partial}{\partial t}\right) v \quad .$$

Therefore, for the transmission line,

$$\frac{\partial^2 v}{\partial x^2} = LG\frac{\partial v}{\partial t} + LC\frac{\partial^2 v}{\partial t^2} \quad ,$$

and for Maxwell's equations,

$$\nabla^2 E = \mu_0\varepsilon_0 \frac{\partial E}{\partial t} + \mu_0\varepsilon_0 \frac{\partial^2 E}{\partial t} \quad ,$$

which is equation (1) without the driver term. If R = 0, the transmission line wave equation is analogous to the equation derived from Maxwell's equations.

5. LUMPED PARAMETER MODEL OF TRANSMISSION LINE

The model of the transmission line used in the design and in the calculated predictions for our experiments is a lumped parameter transmission line consisting of 12 sections. Figure 4 shows the basic section that describes the situation in which the transmission line is pulsed, but the AURORA is not.

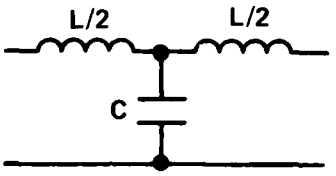

Figure 4. Pulsed transmission line.

The value of the capacitance in farads is determined by the expression

$$C = \varepsilon_0 A/d \quad ,$$

where ε_0 is the permittivity constant, A is the area of the section, and d is the separation of the transmission line.

The value of the inductance, L, was determined by employing equation (15) for the impedance of the transmission line in terms of L and C:

$$Z_0 = \sqrt{\frac{C}{L}} = 90 \quad . \qquad (15)$$

The impedance of the transmission line was determined by the technique of time domain reflectometry. That is to say, the reflection of the transmission line was found to be insignificant when it was terminated with a 90-Ω resistor. We could then use equation (15) to obtain the value of the inductance, or $L = (90)^2 C$. With L and C determined, we were in the position to introduce the effect of time varying air conductivity into a lumped parameter section. The transmission line section was modified to incorporate the effect of a time varying resistor in parallel with the capacitor as shown in figure 5.

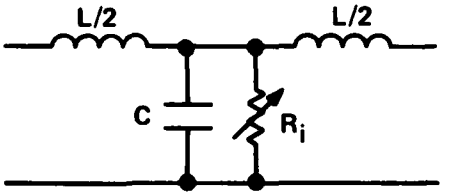

Figure 5. Modified transmission line.

The time varying resistor, R_i, is assumed to vary as

$$\sin^{-2} \{\pi\tau/[\tau + 2 \exp(-\ln 2\, \tau^{\alpha})]\} \text{ rad (Si)/s} \quad ,$$

where

$$\tau = t/t^* \quad ,$$

$$t^* = \text{time of peak},$$

$$\alpha = 1.77\left[A_\gamma^* t^*/\text{dose}\right]^{1.9} \quad ,$$

$$A^* = \text{peak dose rate} \quad .$$

This curve seems to fit a variety of AURORA pulse shapes quite well. It is a smooth curve and lacks the bumps and occasional early time foot seen in some shots. Digitized shot data would be better, but this fit seems adequate. In a few of the calculations not compared with measured data, the simple dependence $\cos^{-2}[\pi(T - T_0/2)]/T_0$ (with $T_0 = 3 \times 10^{-7}$ s) was used.

Air chemistry and air conductivity calculations can be complicated. However, the relatively slow rise time of the AURORA pulse (10 shakes) and the relatively fast attachement rate of electrons to the oxygen component of air at sea level (1 shake) allow us to obtain a simple relationship between the AURORA gamma flux and the resulting air conductivity.

In brief, it can be shown that, in sea level air, the ionization rate of a directed gamma flux is roughly $\dot{\gamma} = 2 \times 10^9 F_\gamma$, where $\dot{\gamma}$ is the ionization rate in ion pairs/cm^{3}s, and F_γ is the directed gamma flux in

roentgens/s. The attachment rate of electrons in sea level air approximately equals 10^{-8} s^{-1}. Since the AURORA gamma flux varies slowly compared with the electron attachment rate, the electron density, N_e, can be estimated by

$$N_e \left(\frac{\text{electrons}}{cm^3}\right) = \frac{\gamma}{\alpha} = 20F_\gamma \quad . \tag{16}$$

In a collision dominated plasma such as partially ionized air at sea level, the air conductivity, σ, is given by

$$\sigma = \frac{e^2 N_e}{m\nu} = eN_e\mu \quad , \tag{17}$$

where m is the electron mass, ν is the collision frequency between free electrons and air molecules, and μ is the electron mobility. Equations (16) and (17) can be combined to yield*

$$\sigma e \left(\frac{\text{mho}}{m}\right) = 5 \times 10^{-14} N_e \tag{18}$$

$$= 0.5 \times 10^{-12} F_\gamma \quad .$$

The gamma flux can be estimated from the total gamma dose and the AURORA pulse shape. The gamma dose is measured with thermoluminescent dosimeters, and the directed flux or the dose rate is then calculated by using the measured AURORA pulse shape. At a later time, after a number of our experiments involving the effect of humidity on the electron mobility have been digested and analyzed, we will allow the electron mobility to be a function of the E-field and the air humidity. In our present analysis, we use the simple relation given in equation (18). If the conductivity, $\sigma_i(T)$, of a transmission line section is known, we can obtain the resistance, $R_i(T)$. Let the area of the transmission line section be A and the distance between the upper and lower conductors be d; then

$$R_i(T) = \frac{d}{\sigma_i(T)A} \quad ,$$

**The value 0.5×10^{-12} F is obtained from Dean May's analysis of our "pie pan" air conductivity measurements. Dean L. May, Electron Mobility and Electron Attachment Rate in an Electromagnetic Pulsed Air Environment, HDL Student Technical Symposium (17-18 August 1977), 87.*

and finally

$$R_i(T) = \frac{d}{\sigma_{maxi} A} \sin^{-2} \{\pi\tau/[\tau + 2 \exp(-\ln 2\, \tau^{\alpha})]\} \quad , \quad (19)$$

where $R_i(T)$ is the time varying resistance across transmission line section i. Figure 5 shows the transmission line section with the time varying resistor across the capacitor to approximate the effect of the time varying conductivity.

Another physical effect has to be incorporated in our model: the effect of the AURORA generated vertical E-field must be superimposed on our transmission line section. It can be superimposed by inserting a current source in parallel with the capacitor and the time varying resistor. The modification is shown in figure 6. As seen in figure 6, the current source consists of a conduction current and a displacement current.

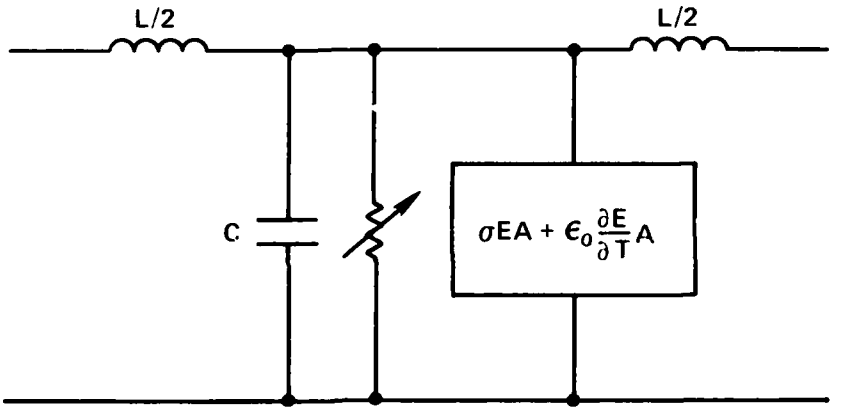

Figure 6. Further modified transmission line.

We previously described our measurement of the values of the vertical E-field and dE/dt produced in the "empty" AURORA test cell (the AURORA test cell without the transmission line) when the AURORA is fired. The E-field used in our current source is shown in figure 2.

We can now write the series of voltage and current first-order differential equations that describe the transmission line, but first let us consider how the first transmission line section is connected to the pulser: A low inductance 2-μF capacitor is discharged into the

transmission line as shown in figure 7. To be consistent with our Runge-Kutta subroutine, we label the voltages with odd numbers and the currents with even numbers. In other words, the voltage at node N is designated V(2N - 1), and the current flowing in the line into node N is labeled I(2N). The advantages of this method of notation are clear when we consider the actual node equations to be solved by the Runge-Kutta method.

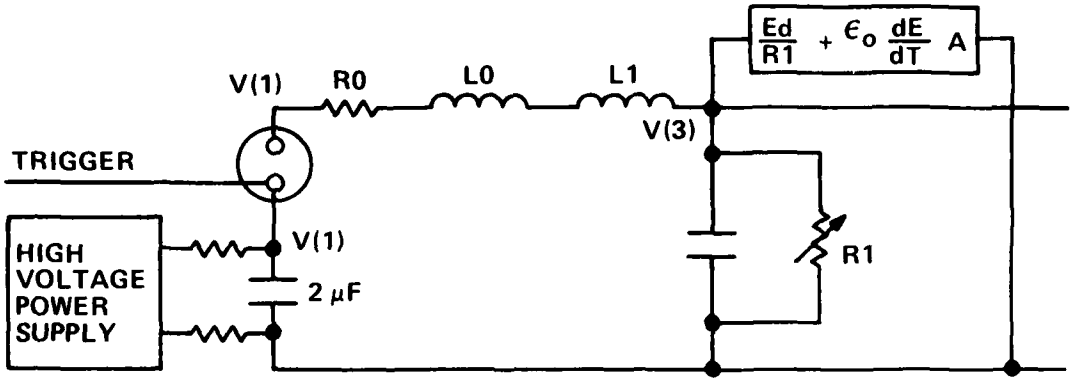

Figure 7. Discharge into transmission line.

Let us consider the partial circuit shown in figure 7. Three of the *first current and voltage equations are*

$$C0 \frac{dV(1)}{dT} = -I(2) \quad , \tag{20}$$

$$L1 \frac{dI(2)}{dT} = V(1) - V(3) - R0 \times I(2) \quad , \tag{21}$$

$$C1 \frac{dV(3)}{dT} = - \frac{V(3)}{R1(T)} + I(2) - I(4) + \frac{ABC}{R1(T)} + (DABC) \quad , \tag{22}$$

where

$$ABC = Ed, \tag{23}$$

$$DABC = \epsilon_0 \frac{dE}{dT} A \quad . \tag{24}$$

The values of E and dE/dT in equations (23) and (24) are given by equations (25) (multiexponential field) and (26), respectively. The values of the constants in equations (25) and (26) were obtained by the curve fit shown in figure 3. In our first application of the code, we assume that E and dE/dT are constant along the transmission line. We do, however, allow the value of $\sigma_i(T)$ or $R_i(T)$ to be determined by the radiation dose along the transmission line.

$$E(T) = (A1 - A2)(1 + \eta T)e^{-\eta T} + (A2 + A3)(1 + \beta T)e^{-\beta T}$$

$$- A1(1 + \alpha T)e^{-\alpha T} - A3(1 + \gamma T)e^{-\gamma T}$$

$$+ A4\ U(T - T')\{[1 + \beta'(T - T')]e^{-\beta'(T-T')} \qquad (25)$$

$$- [1 + \alpha'(T - T')]e^{-\alpha'(T-T')}\}$$

$$\frac{dE(T)}{dT} = A1\ \alpha^2 Te^{-\alpha T} + A3\ \gamma^2 Te^{-\gamma T}$$

$$- (A1 - A2)\eta^2 Te^{-\eta T} - (A2 + A3)\beta^2 Te^{-\beta T}$$

$$- A4\ U(T - T')\left((\beta')^2(T - T')e^{-\beta'(T-T')}\right. \qquad (26)$$

$$\left. - (\alpha')^2(T - T')e^{-\alpha'(T-T')}\right) \quad .$$

Figure 8 shows the circuit for the termination end of the transmission line.

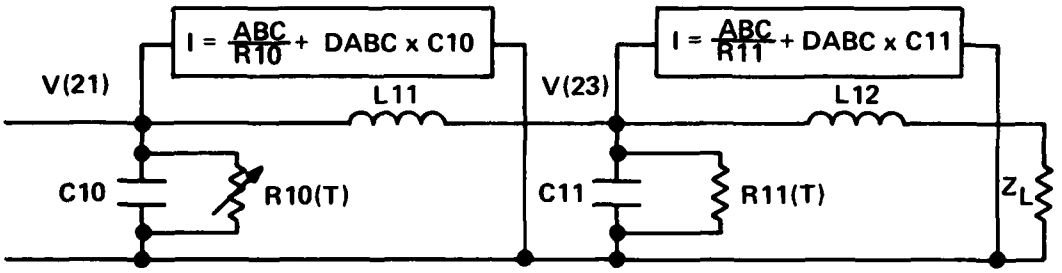

Figure 8. Termination of transmission line.

The current sources $I_i = E \cdot d/R_i + \varepsilon_0 A(dE/dT)$ vary as a function of position along the transmission line because R_i varies as a function of radiation dose. In a more accurate calculation, E and dE/dT would most likely vary. Also, R_i would be a function of dose and E-field because mobility varies as a function of E. The effect of the variation of A in the tapered sections of the transmission line would affect also the value of the displacement current, $\varepsilon_0 A(dE/dT)$.

The 24 differential equations that describe the lumped parameter model of the transmission line are given in table I (p. 22). The table is actually a portion of the Runge-Kutta FORTRAN subroutine.

6. TRANSMISSION LINE EXPERIMENTS

6.1 Physical Description of Transmission Line

The transmission line was fired with three different pulser configurations (fig. 9 to 11).

Figure 12 shows a schematic view of the transmission line, and an alteration of the transmission line configuration was to shield the tapered ends of the transmission line with a lead brick wall. The purpose of the lead shield was to cut down the ionization of the air in the tapered sections of the line and to deliver as much E-field and energy to the nontapered sections of the transmission line as possible. Various configurations of the transmission line with and without lead shields are shown in figure 13.

TABLE I. EQUATIONS TO SOLVE TRANSMISSION LINE TERMINATED IN 90-Ω RESISTANCE

```
F(1) =-Y(2)/C0
F(2) = Y(1)/L1-Y(3)/L1  -(R0/L1)*Y(2)
F(3) =  -Y(3)/( R1*C1)  +Y(2)/C1  -Y(4)/C1 + ABC/(R1*C1) + DABC
F(4) = Y(3)/L2 - Y(5)/L2
F(5) = -Y(5)/(C2*R2) + Y(4)/C2 - Y(6)/C2   + ABC/(C2*R2) + DABC
F(6) = Y(5)/L3 - Y(7)/L3
F(7) = - Y(7)/(C3*R3) + Y(6)/C3 - Y(8)/C3 + ABC/(C3*R3)  + DABC
F(8) = Y(7)/L4 - Y(9)/L4
F(9) = -Y(9)/(C4*R4) + Y(8)/C4 - Y(10)/C4  + ABC/(C4*R4) + DABC
F(10) = Y(9)/L5 - Y(11)/L5
F(11) = -Y(11)/(C5*R5) + Y(10)/C5 -Y(12)/C5 + ABC/(C5*R5)+ DABC
F(12) = Y(11)/L6 - Y(13)/L6
F(13) = -Y(13)/(C6*R6) + Y(12)/C6 -Y(14)/C6  + ABC/(C6*R6) + DABC
F(14) = Y(13)/L7 - Y(15)/L7
F(15) = -Y(15)/(C7*R7) + Y(14)/C7 - Y(16)/C7  + ABC/(C7*R7)
1  + DABC
F(16) = Y(15)/L8 - Y(17)/L8
F(17) = -Y(17)/(C8*R8) + Y(16)/C8  - Y(18)/C8  + ABC/(C8*R8)
1  + DABC
F(18) = Y(17)/L9 -Y(19)/L9
F(19) = -Y(19)/(C9*R9) + Y(18)/C9 -Y(20)/C9   + ABC/(C9*R9)
1  + DABC
F(20) = Y(19)/L10-Y(21)/L10
F(21) = -Y(21)/(C10*R10)+Y(20)/C10-Y(22)/C10  + ABC/(R10*C10)
1  + DABC
F(22) = Y(21)/L11-Y(23)/L11
F(23) = -Y(23)/(C11*R11)+Y(22)/C11-Y(24)/C11  + ABC/(C11*R11)
1  + DABC
F(24) = Y(23)/L12 -Y(24)*(R12/L12)
```

Note: Let N refer to node N,
dV(N)/dT = F(2N-1),
V(N) = Y(2N-1)
dI(N)/dT = F(2N),
I(N) = Y(2N),
where I(N) is the current flowing into node N.

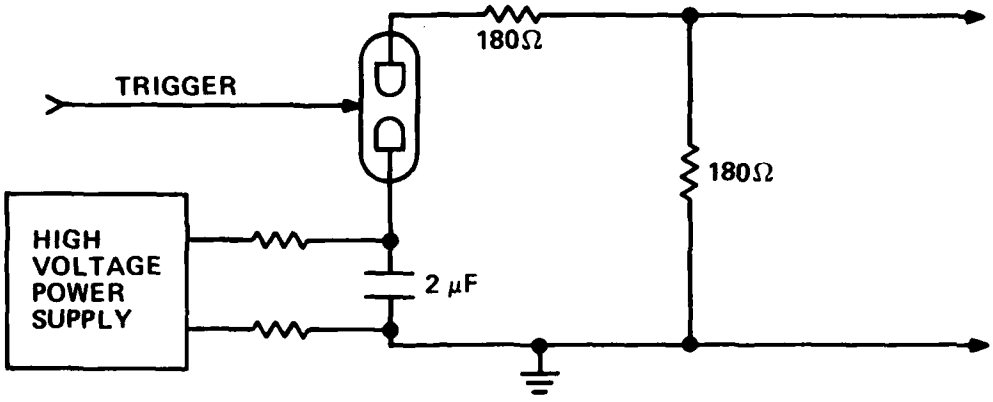

Figure 9. Pulser configuration I.

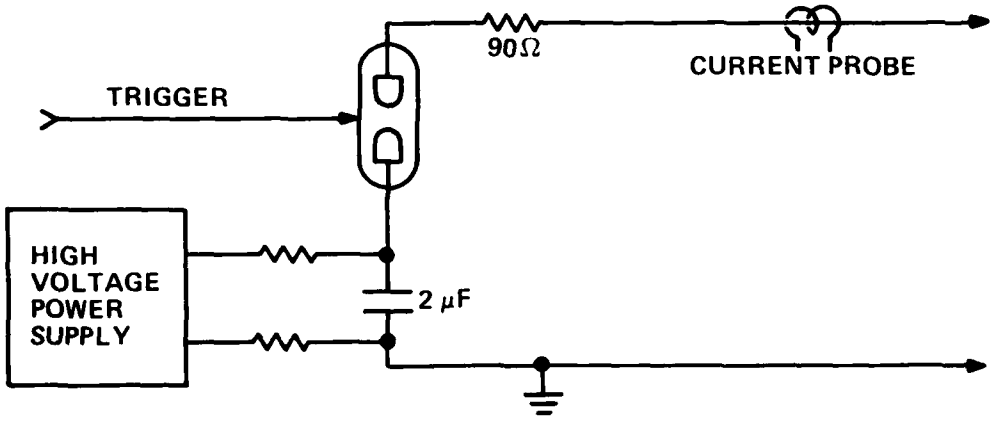

Figure 10. Pulser configuration II.

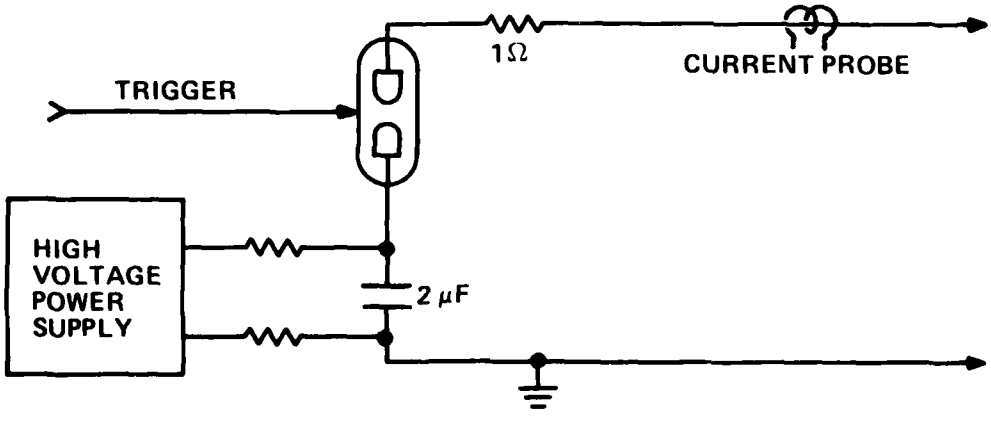

Figure 11. Pulser configuration III.

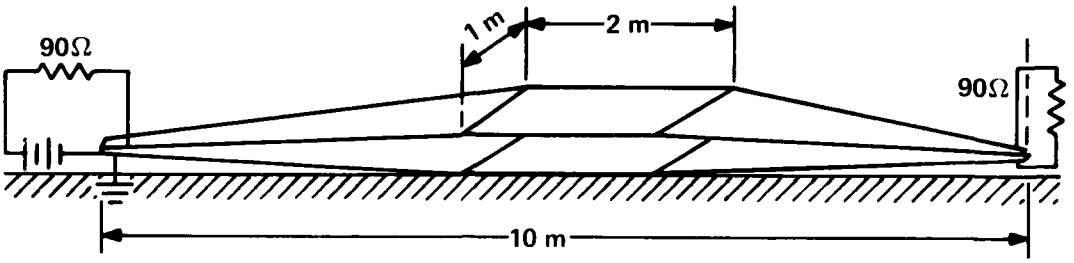

Figure 12. Transmission line configuration (central 2-m-long section is 0.4 m high; resistors correspond to configuration II).

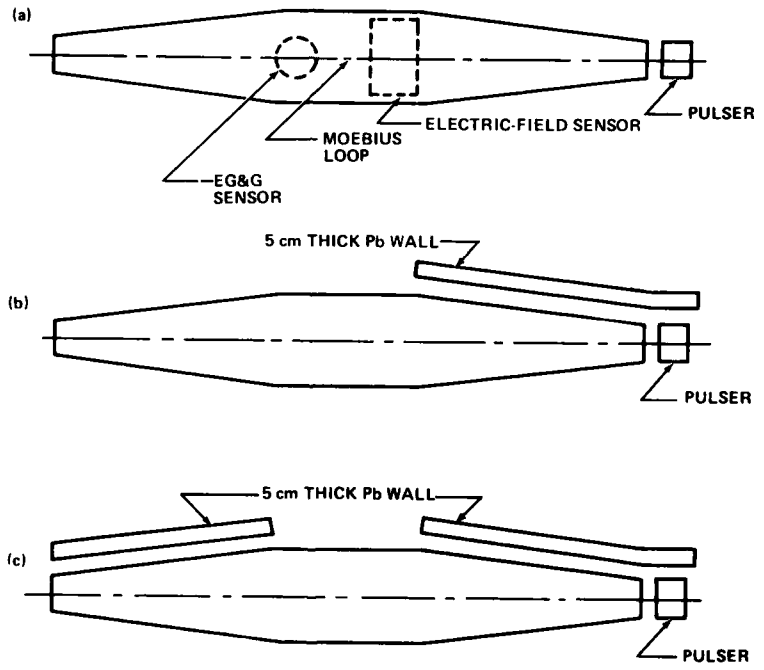

Figure 13. Top view of ionizing radiation shielding configurations: (a) no shielding, (b) tapered section shielded near pulser, and (c) both tapered sections shielded.

6.2 Experimental Measuring Techniques

A number of parameters were measured during each AURORA shot involving the transmission line. Two E-field sensors were placed in the parallel section of the transmision line. One sensor was the Air Force Weapons Laboratory (AFWL) EG&G PMD-1 sensor designed by Carl Baum; the other was a parallel plate sensor that fed into a high impedance input emitter follower to increase the sensor time constant. Its general design was suggested by van Lint. At the center of the transmission line, a Moebius loop was installed to measure the H-field. Current into the transmission line and current at the matched termination were measured with ionizing radiation insensitive Adelco current probes.

7. COMPARISON OF EXPERIMENT AND CALCULATION

Four electromagnetic parameters were measured with each simultaneous firing of the AURORA for the transmission line. These experimental parameters were the E-field at the center of the transmission line, the H-field at the center of the transmission line, the current at the termination of the transmission line, and the current at the input of the transmission line. We measured also the total ionizing radiation dose at various points along the transmission line. For this report, we only digitized our data and corrected them with a measured transfer function. We did not apply all possible corrections and refinements to our theory. Air conductivity refinements such as humidity and radiation dose variations from shot to shot were left for later consideration. Also, a few systematic errors needed to be resolved.

7.1 Measured Electric Field and Calculated Transmission Line Voltage

7.1.1 Configuration I

The E-field in the transmission line was measured with the AFWL EG&G E-field sensor and with an E-field sensor designed by van Lint. Since the parallel transmssion line separation was 0.4 m, the transmission line voltage is given by $V = 0.4E$. Figure 14 compares the calculated and measured E-fields across the untapered portion of the transmission line for impedance matching configuration I when the transmission line pulser was not pulsed; the voltage across the transmission line section was caused only by the AURORA generated electromagnetic field in the AURORA test cell.

Figure 15 compares the calculated and measured E-fields for experimental configuration I when the pulser capacitor was charged to 6000 V and discharged a few micrseconds before the AURORA was fired.

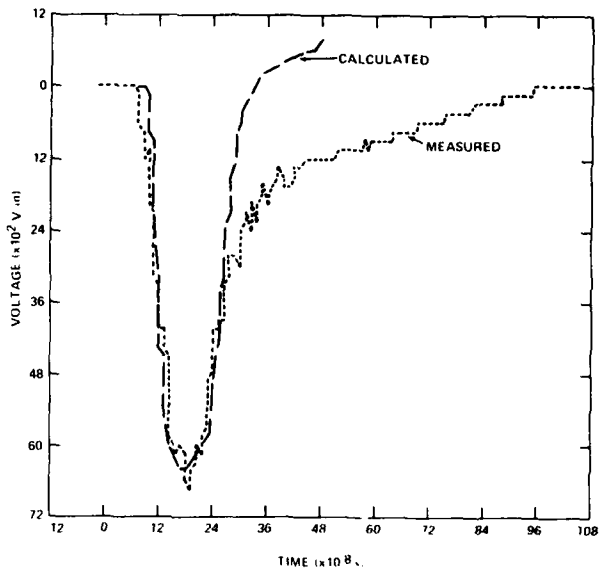

Figure 14. Electric field, transmission line pulser not pulsed, configuration I.

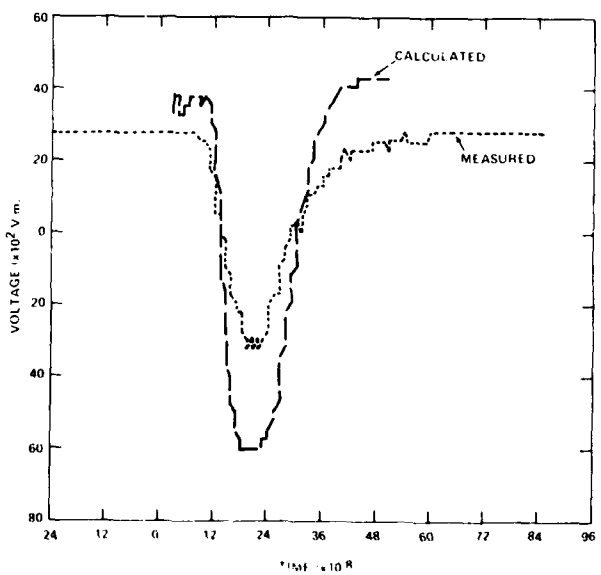

Figure 15. Electric field, transmission line pulser pulsed, configuration I.

7.1.2 Configuration II

Figure 16 shows the calculated and measured E-field across the untapered portion of the transmission line for impedance matching configuration II. The transmission line pulser was not pulsed so that the voltage appearing across the transmission line was caused only by the AURORA generated electromagnetic field in the AURORA test cell.

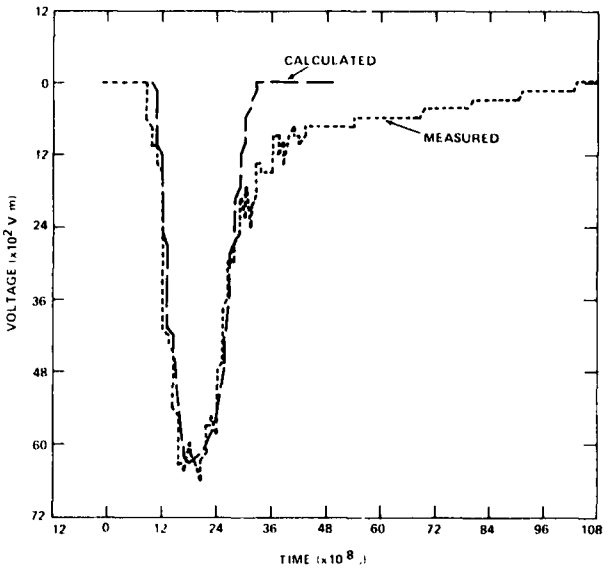

Figure 16. Electric field, transmission line pulser not pulsed, configuration II.

Figure 17 compares the calculated and measured E-fields for experimental configuration II, except that the transmission line capacitor was charged to 4000 V and discharged a few microseconds before the AURORA was fired.

Figure 18 shows a purely calculated result. The transmission line was assumed to be in impedance matching configuration II, and the electromagnetic field in the AURORA test cell was assumed to be zero, but the ionizing radiation was assumed to be present. The transmission line capacitor was assumed to be charged to 4000 V, and the pulser was assumed to be discharged about 100 ns before the AURORA was fired.

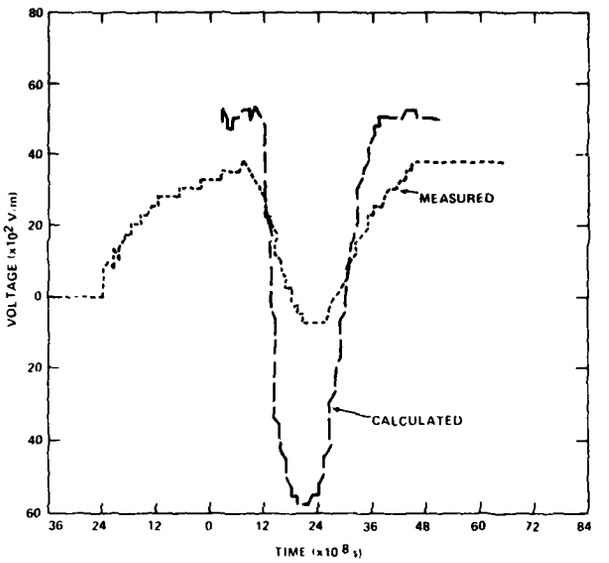

Figure 17. Electric field, transmission line pulser pulsed, configuration II.

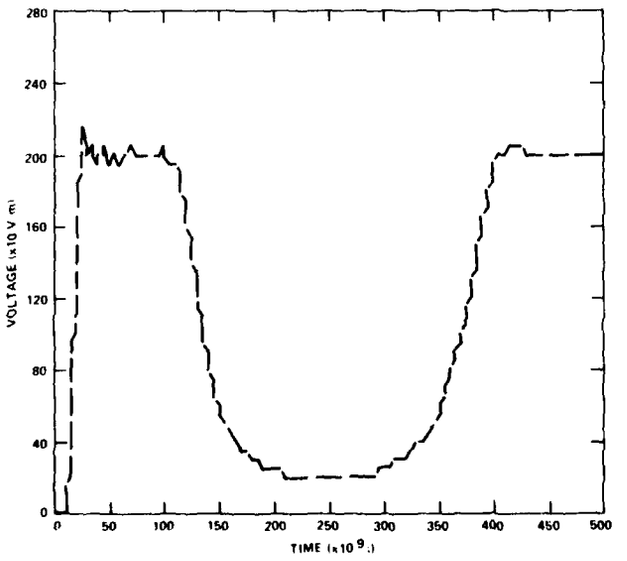

Figure 18. Calculated electric field, transmission line pulser discharged, configuration II.

7.1.3 Configuration III

When the transmission line tapered sections were not shielded with lead, the unreliability of both the trigger circuit and the accompanying trigatron interfered with measurements for impedance matching configuration III. To not exceed the dynamic range of the E-field measuring electronics, the transmission line capacitor was not charged beyond 2000 V. Unfortunately, the triggering circuit and the trigatron could not reliably operate at such a low voltage. However, two interesting calculational results correspond to configuration III.

Figure 19 shows the calculated behavior of the transmission line when the measured E-field in the AURORA test cell is taken into consideration. The large late time spike occurs whenever the impedance matching network does not limit the current that can flow into the transmission line. A possible explanation for the spike is that the ionizing radiation short-circuits the transmission line, and the resulting large current produces a large H-field and an accompanying large magnetic energy in the line. When the ionizing radiation disappears, some of the magnetic energy is converted into electrical energy, and a large voltage is produced across the transmission line.

The results shown in figure 20 are similar to the results shown in figure 19, except that the E-field produced by the AURORA in the test cell is not included in the figure 20 calculation.

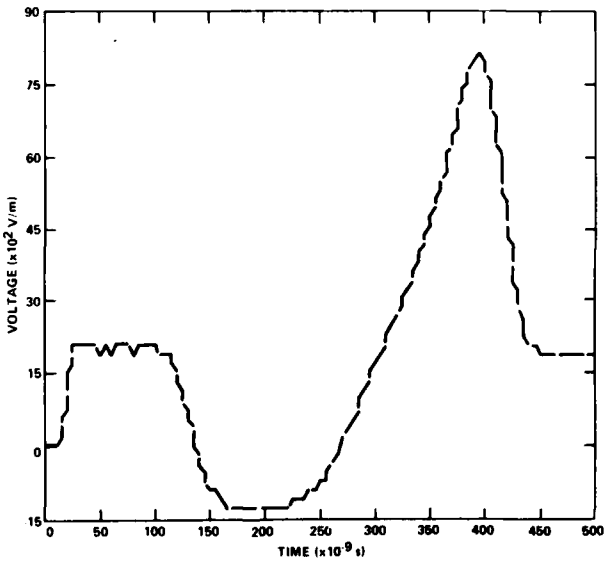

Figure 19. Calculated electric field of transmission line, configuration III.

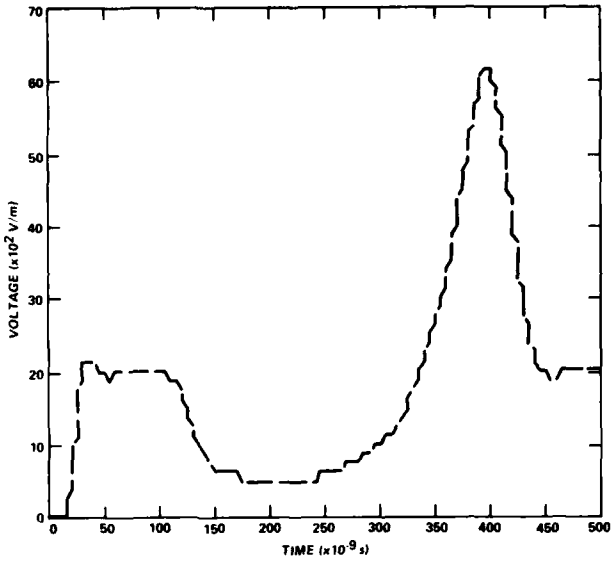

Figure 20. Calculated electric field, transmission line, configuration III (AURORA electric field not included).

7.2 Experimental Measurements with Lead Shielding in Place

Figure 21 compares the calculated and measured E-fields for impedance matching configuration I; the transmission line was pulsed with 6000 V, and the tapered section of the transmission line near the pulser was shielded with lead. Figure 22 compares the calculated and measured E-fields for a configuration II impedance match; the transmission line was pulsed 4000 V, and the tapered section near the pulser was shielded with lead. Figure 17 shows the equivalent unshielded result. Figure 23 compares the calculated and measured E-fields for a configuration II impedance match. The AURORA and the transmission line pulser were fired at approximately the same time. For this measurement, the tapered transmission line transition sections both near the pulser and next to the termination were shielded with 2-in. (5.08-cm) lead shield walls.

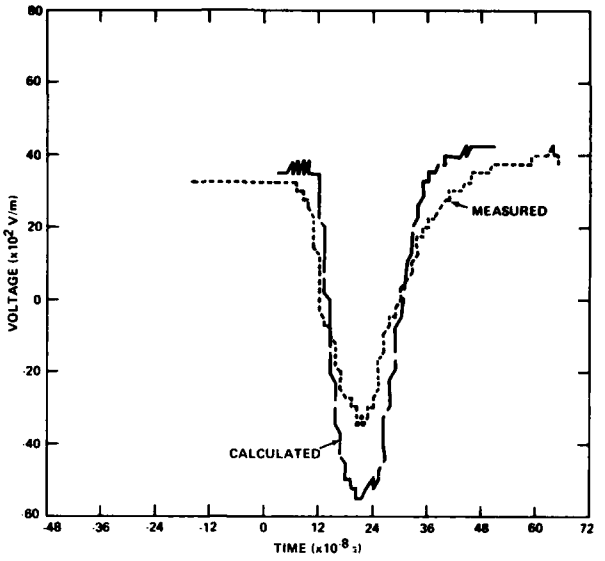

Figure 21. Calculated and measured electric fields, transmission line, configuration I.

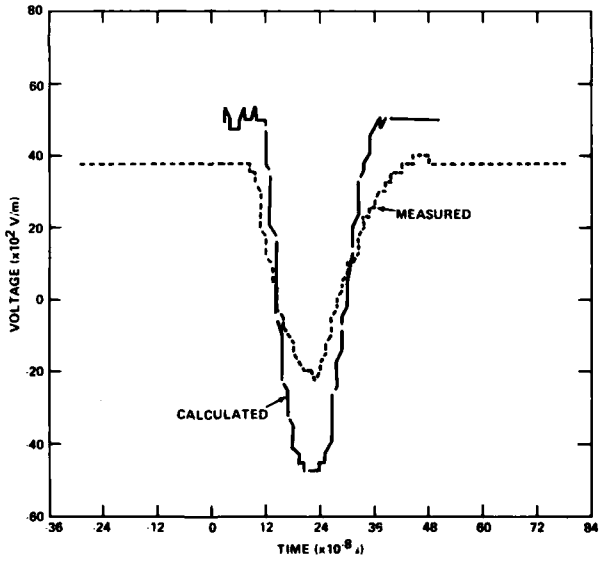

Figure 22. Calculated and measured electric fields, transmission line, configuration II.

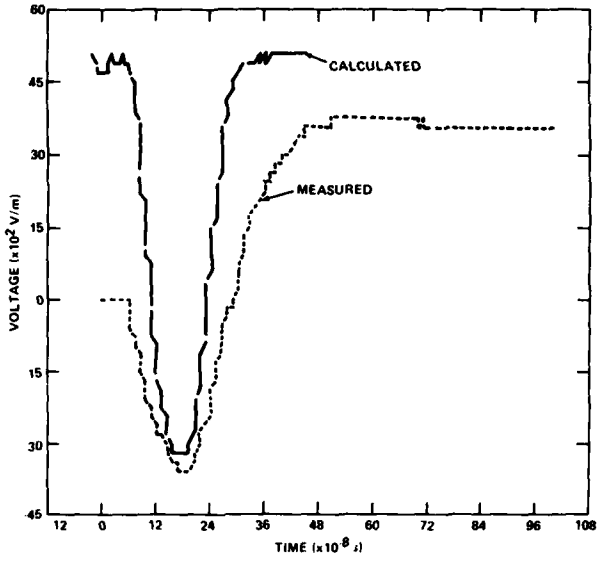

Figure 23. Calculated and measured electric fields, transmission line, configuration II (AURORA and pulser fired at approximately same time).

7.3 Measured and Calculated Input Currents

The lumped parameter code also can be used to calculate the current into the transmission line at the points indicated in figures 10 and 11.

Figure 24 compares the calculated and measured input currents to the transmission line for input impedance matching configuration II. Figure 25 compares the input current and the calculated current for input configuration III. Figure 24 corresponds to the unshielded shot, and figure 25 corresponds to the shot in which both tapered ends of the transmission line are shielded with lead. The model predicts the input current to within 50 percent.

7.4 Measured and Calculated Termination Currents

Figure 26 compares the calculated and measured termination currents for transmission line pulser impedance matching configuration I with the transmission line pulser capacitor charged to 6 kV. Figure 27 compares the calculated and measured termination currents for impedance matching termination configuration I, but with the transmission line pulser capacitor charged to 0 V.

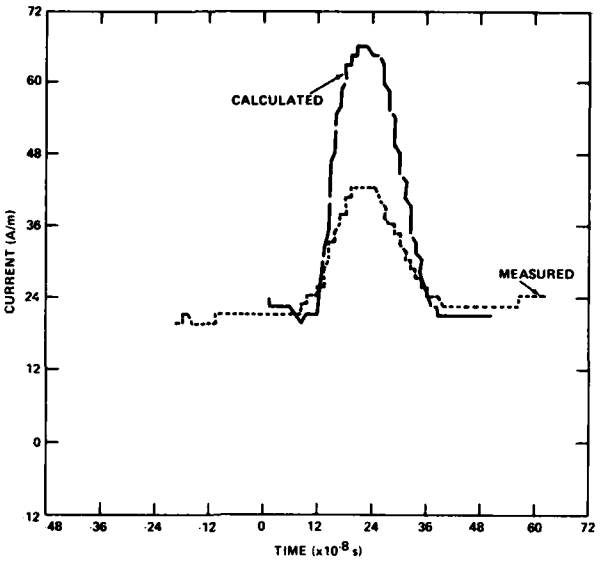

Figure 24. Calculated and measured input currents, transmission line, configuration II.

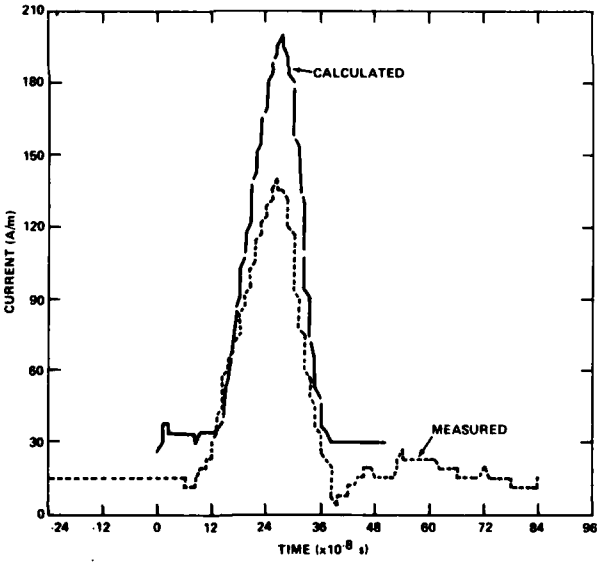

Figure 25. Calculated and measured input currents, transmission line, configuration III.

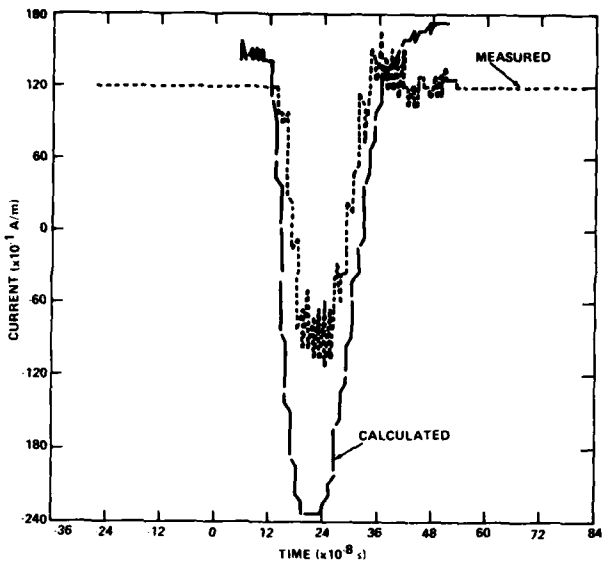

Figure 26. Calculated and measured termination currents, transmission line, configuration I (capacitor 6 kV).

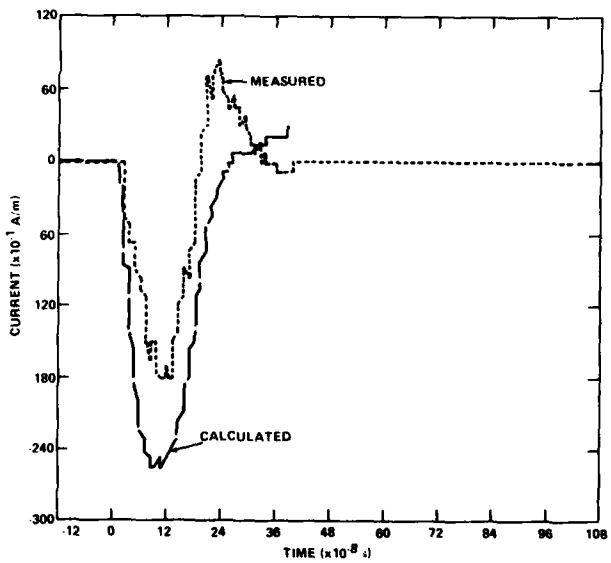

Figure 27. Calculated and measured termination currents, transmission line, configuration I (capacitor 0 V).

Figure 28 shows the calculated and measured termination currents for pulser impedance matching configuration II with the transmission line pulser capacitor charged to 4 kV. Figure 29 shows the calculated and measured termination currents for impedance matching configuration II with the capacitor charged to 0 V.

Figure 30 compares the calculated and measured termination currents for pulser impedance matching configuration III. Figure 30 corresponds to an experimental setup with the tapered section of the transmission line near the pulser shielded with a 5.08-cm lead wall. The reason that we were able to obtain these results is that the pulser was charged to 3 kV. This high voltage saturated the E-field sensor, but allowed us to synchronize the transmission line pulse with the AURORA pulse. The pattern emerging from figures 26 to 30 is that our lumped parameter model of the transmission line is a qualitative and even semiquantitative prediction of the actual measured termination current.

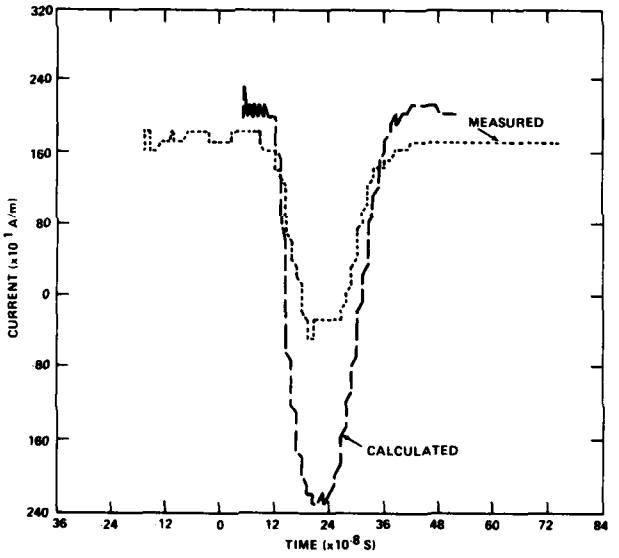

Figure 28. Calculated and measured termination currents, transmission line, configuration II (capacitor 4 kV).

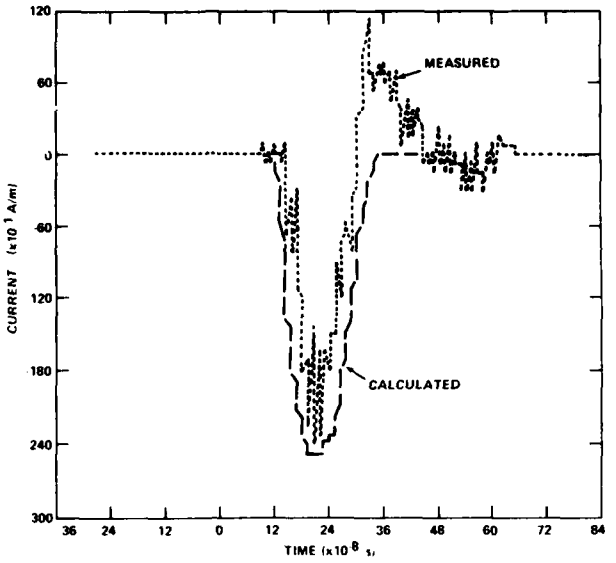

Figure 29. Calculated and measured termination currents, transmission line, configuration II (capacitor 0 V).

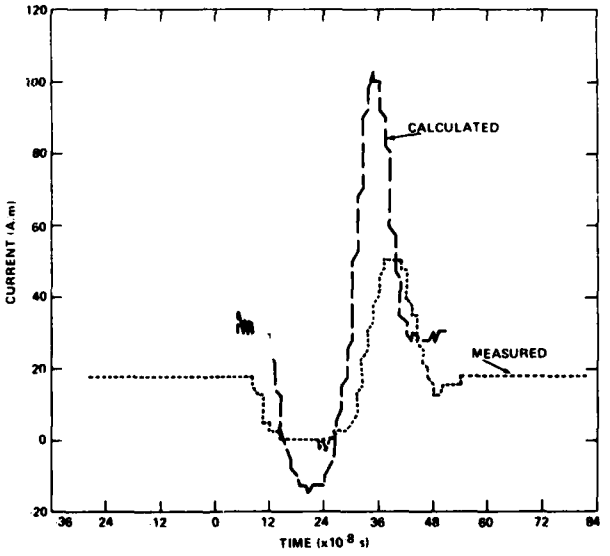

Figure 30. Calculated and measured termination currents, transmission line, configuration III.

7.5 Magnetic Field Measurement

The Moebius loop H-field sensor was oriented so that it would measure the H-field produced by the current flowing along the transmission line. Unfortunately, only one Moebius loop was positioned in the transmission line, and it was at one half the distance between the transmission line pulser and the transmission line termination. Although it probably would have been more informative if we had had many H-field sensors distributed along the transmission line, the number of data channels and oscilloscopes limited their placement.

According to our lumped parameter model, the shape of the voltage pulse does not vary appreciably from node to node; however, the shape of the current pulse does vary appreciably from the transmission line pulser to the termination. The explanation may be found in terms of the general transmission line equation:

$$\frac{\partial v}{\partial x} = -\left(R + L\frac{\partial}{\partial t}\right) i \quad , \tag{27}$$

$$\frac{\partial i}{\partial x} = -\left(G + C\frac{\partial}{\partial t}\right) v \quad ,$$

where R, L, C, and G are shown in figure 31. Usually, R and G are very small, and the transmission line equation for a coaxial line then reduces to the familiar form

$$\frac{\partial^2 v}{\partial x^2} = LC\frac{\partial v^2}{\partial t^2} \quad ,$$

$$\frac{\partial^2 i}{\partial x^2} = LC\frac{\partial^2 v}{\partial t^2} \quad .$$

In our experiment, G is a current sink that drains off current as we progress along the line. We have not only a current sink, but also a current source in parallel with the sink (sect. 5).

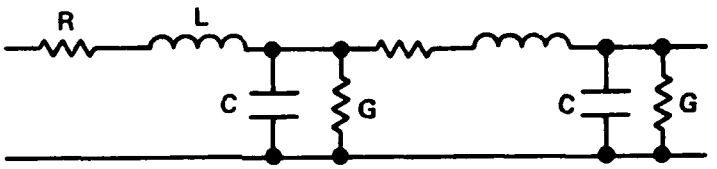

Figure 31. Schematic of transmission line.

Another more succinct drawing of a section of a lumped parameter transmission line is shown in figure 32. In this line,

$$Z = R + L \frac{\partial}{\partial t} \text{ (ohm/m)} \quad ,$$

and

$$Y = G + C \frac{\partial}{\partial t} \text{ (mho/m)} \quad .$$

Figure 32 depicts an approximate model. There are ways of obtaining an exact model for a section of line at a single frequency, but we are working in the time domain.

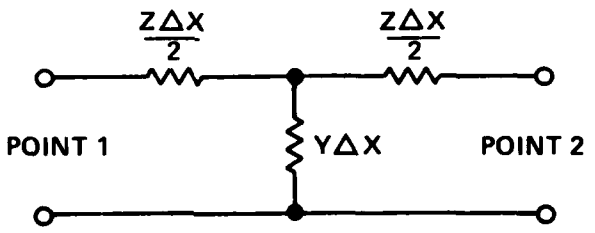

Figure 32. Lumped parameter transmission line.

A model with the above approximate sections is a reasonably good representation of a transmission line, provided that the voltage drop between points 1 and 2 is small compared with the voltage across the line at either end of the section and that the loss in current through the shunt admittance is small compared with the total current flowing in the line. That is,

$$V_2 - V_1 \ll V_1 \quad ,$$

and

$$I_2 - I_1 \ll I_1 \quad .$$

The first voltage inequality was met in our calculations and measurements. However, the current inequality was met only marginally. Our H-field measurements were intrinsically related to the current in the line. From a theoretical point of view, we most probably can improve our model by increasing the number of sections in the lumped parameter model. Ultimately, as the number of sections is increased, both inequalities will be met. This matter can be investigated by computer experiments in which the number of sections is increased.

Consider the transmission line in the case of a pulser impedance match of type I with the pulser capacitor charged to 6 kV. Figures 33 and 34 show the voltage and the current at node 2, and figures 35 and 36 show the voltage and the current at termination node 12. The voltage pulses at nodes 2 and 12 are quite similar, but the current pulses are quite different. Figure 37 plots the current maximum or minimum during the AURORA pulse as a function of node number or position along the line. Figure 37 emphasizes the variation of current pulse shape as a function of position along the line.

Figure 38 compares the variation of the current inferred from the Moebius loop and the calculated current flowing into node 7. In general, we can say that figure 38 shows fairly good agreement between calculation and measurement. However, a more definitive comparison with H-fields along the transmission line and our lumped parameter theory would require a number of Moebius loops spaced along the transmission line rather than just one loop halfway between the pulser and the termination.

Figures 39 and 40 are calculated currents for nodes 6 and 7 for the capacitor charged to 0 V and the pulser matching circuit of configuration II. The current changes sign near the center of the line for this configuration and capacitor voltage; thus, it is a poor position for our single Moebius loop.

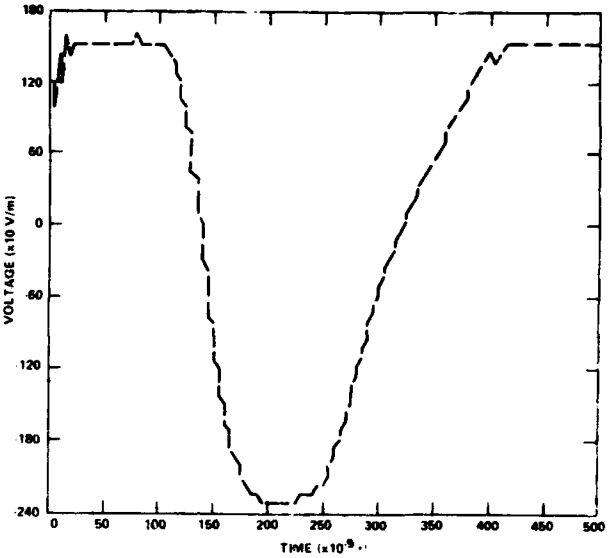

Figure 33. Voltage at node 2.

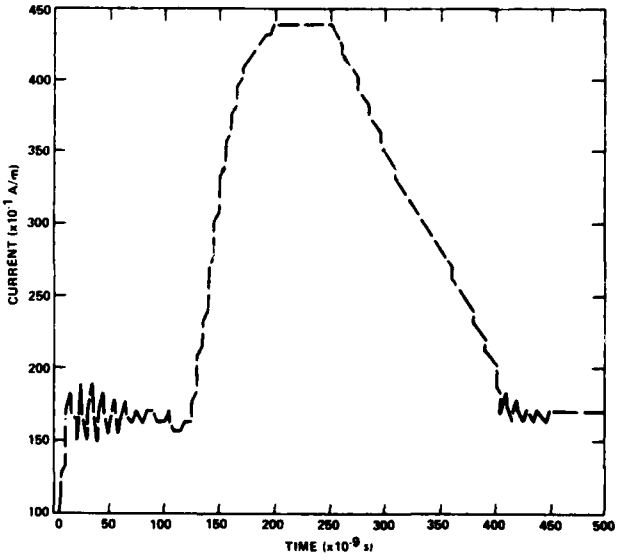

Figure 34. Current at node 2.

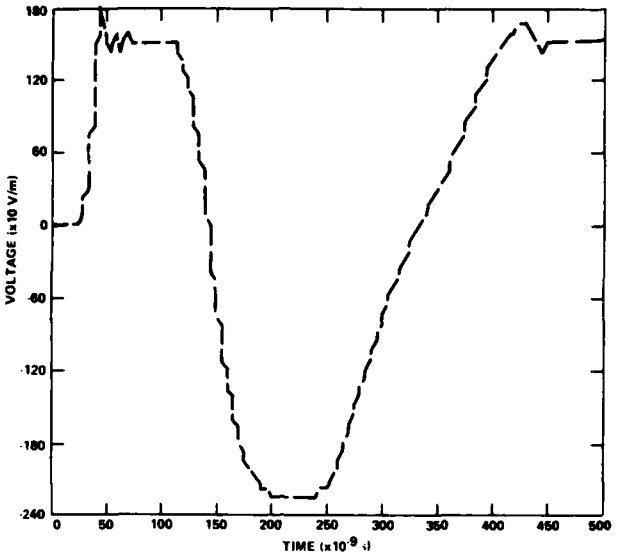

Figure 35. Voltage at termination node 12.

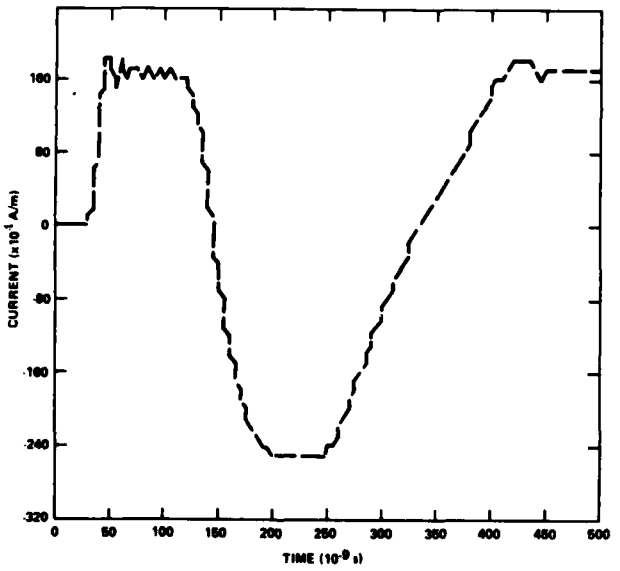

Figure 36. Current at termination node 12.

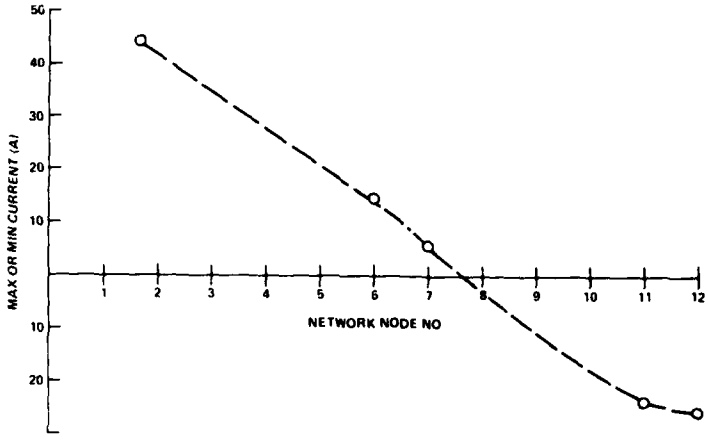

Figure 37. Current during AURORA pulse.

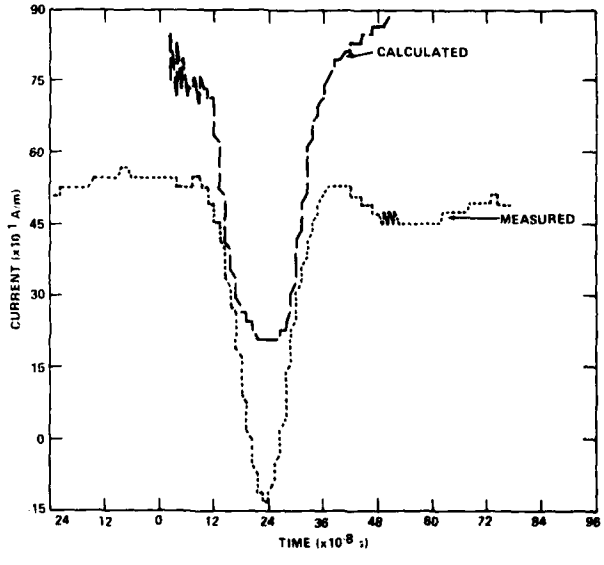

Figure 38. Calculated and measured current into node 7.

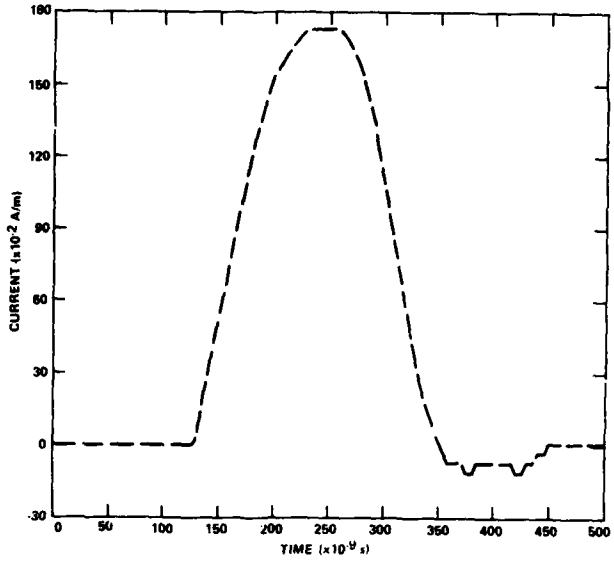

Figure 39. Calculated current into node 6.

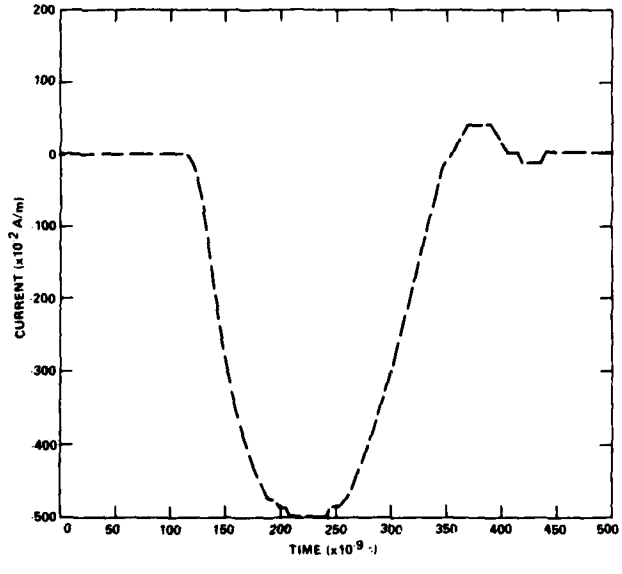

Figure 40. Calculated current into node 7.

8. CONCLUSIONS

This report describes a series of experiments in which a parallel plate transmission line was used to augment the electromagnetic field in the AURORA test cell during an AURORA shot. A simple lumped parameter model of the transmission line was modified with time varying resistors and with parallel current sources. This model is a good tool to use to understand the many aspects of the behavior of the line when subjected to the time varying ionizing radiation produced by the AURORA firing. A more sophisticated calculation is being developed for the time varying resistances across the transmission line during an AURORA shot. When results obtained from that experiment are compared with the finally analyzed measurements, the agreement may very well become closer. We are confident that our transmission line theory gives a qualitative, even semiquantitative description of the superposition of a vertical E-field upon the conducting ionized air by the transmission line. The next task is to use this simple transmission line model to determine whether or not to modify the AURORA test cell environment so that it more closely resembles that associated with the actual tactical source region.

DISTRIBUTION

DEFENSE DOCUMENTATION CENTER
CAMERON STATION, BUILDING 5
ALEXANDRIA, VA 22314
ATTN DDC-TCA (12 COPIES)

COMMANDER
USA RSCH & STD GP (EUR)
BOX 65
FPO NEW YORK 09510
ATTN LTC JAMES M. KENNEDY, JR.
CHIEF, PHYSICS & MATH BRANCH

COMMANDER
US ARMY MATERIEL DEVELOPMENT
& READINESS COMMAND
5001 EISENHOWER AVENUE
ALEXANDRIA, VA 22333
ATTN DRXAM-TL, HQ TECH LIBRARY

COMMANDER
US ARMY ARMAMENT MATERIEL
READINESS COMMAND
ROCK ISLAND ARSENAL
ROCK ISLAND, IL 61299
ATTN DRSAR-LEP-L, TECHNICAL LIBRARY

COMMANDER
USA MISSILE & MUNITIONS
CENTER & SCHOOL
REDSTONE ARSENAL, AL 35809
ATTN ATSK-CTD-F

DIRECTOR
US ARMY MATERIEL SYSTEMS
ANALYSIS ACTIVITY
ABERDEEN PROVING GROUND, MD 21005
ATTN DRXSY-MP
ATTN DRXSY-CC
ATTN DRXSY-PO

DIRECTOR
US ARMY BALLISTIC RESEARCH LABORATORY
ABERDEEN PROVING GROUND, MD 21005
ATTN DRDAR-TSB-S (STINFO)

TELEDYNE BROWN ENGINEERING
CUMMINGS RESEARCH PARK
HUNTSVILLE, AL 35807
ATTN DR. MELVIN L. PRICE, MS-44
ATTN FRED LEONARD

US ARMY ELECTRONICS TECHNOLOGY
& DEVICES LABORATORY
FORT MONMOUTH, NJ 07703
ATTN DELET-DD

DIRECTOR
ARMED FORCES RADIOBIOLOGY
RESEARCH INSTITUTE
DEFENSE NUCLEAR AGENCY
NATIONAL NAVAL MEDICAL CENTER
BETHESDA, MD 20014
ATTN RPC
ATTN TECHNICAL LIBRARY

ASSISTANT TO THE SECRETARY OF DEFENSE
ATOMIC ENERGY
DEPARTMENT OF DEFENSE
WASHINGTON, DC 20301
ATTN STAFF ASST (R&D)

DIRECTOR
DEFENSE ADVANCED RSCH PROJ AGENCY
ARCHITECT BUILDING
1400 WILSON BLVD.
ARLINGTON, VA 22209
ATTN TECHNICAL LIBRARY
ATTN AD/E&PS

DIRECTOR
DEFENSE CIVIL PREPAREDNESS AGENCY
ASSISTANT DIRECTOR FOR RESEARCH
WASHINGTON, DC 20301
ATTN TS(AED)
ATTN RE(EO)
ATTN ADMIN OFFICER
ATTN PO(SE)

DEFENSE COMMUNICATIONS
ENGINEERING CENTER
1860 WIEHLE AVENUE
RESTON, VA 22090
ATTN CODE R720, C. STANSBERRY
ATTN CODE R400
ATTN CODE R123, TECH LIB

DIRECTOR
DEFENSE COMMUNICATIONS AGENCY
WASHINGTON, DC 20305
ATTN CODE 930,
MONTE I. BURGETT, FR
ATTN CCTC C312
ATTN CCTC/C672
ATTN CCTC C313

GSA/FPA
GS BLDG, 18TH & F STS NW
WASHINGTON, DC 20405
ATTN EGT

COMMANDER
DEFENSE ELECTRONIC SUPPLY CENTER
1507 WILMINGTON PIKE
DAYTON, OH 45401
ATTN ECS
ATTN ROSS V. DOUGHTY
ATTN EQ

DIRECTOR
DEFENSE INTELLIGENCE AGENCY
WASHINGTON, DC 20301
ATTN RDS-3A
ATTN DB-4C, EDWARD OFARRELL
ATTN RDS-3A4, POMPONIO PLAZA

DIRECTOR
DEFENSE NUCLEAR AGENCY
WASHINGTON, DC 20305
ATTN RATN
ATTN DDST
ATTN RAEV
ATTN TITL TECH LIBRARY
ATTN TISI ARCHIVES
ATTN STVL
ATTN RAAE

UNDER SECRETARY OF DEFENSE
FOR RESEARCH & ENGINEERING
DEPARTMENT OF DEFENSE
WASHINGTON, DC 20301
ATTN S&SS(OS)
ATTN G. BARSE

COMMANDER
FIELD COMMAND
DEFENSE NUCLEAR AGENCY
KIRTLAND AFB, NM 87115
ATTN FCPR
ATTN FCSM-F3/CDR SMITH
ATTN FCLMC

DIRECTOR
INTERSERVICE NUCLEAR WEAPONS SCHOOL
KIRTLAND AFB, NM 87115
ATTN DOCUMENT CONTROL

DIRECTOR
JOINT STRATEGIC TARGET PLANNING
STAFF, JCS
OFFUTT AFB
OMAHA, NB 68113
ATTN STINFO LIBRARY
ATTN JSAS
ATTN JLTW-2

CHIEF
LIVERMORE DIVISION, FIELD COMMAND DNA
LAWRENCE LIVERMORE LABORATORY
P.O. BOX 808
LIVERMORE, CA 94550
ATTN FCPRL

NATIONAL COMMUNICATIONS SYSTEM
OFFICE OF THE MANAGER
WASHINGTON, DC 20305
ATTN NCS-TS, CHARLES D. BODSON

DIRECTOR
NATIONAL SECURITY AGENCY
FT. GEORGE G. MEADE, MD 20755
ATTN O. O. VAN GUNTEN, R-425
ATTN TECHNICAL LIBRARY
ATTN R522
ATTN T1213
ATTN TDL
ATTN T412

OJCS/J-3
THE PENTAGON
WASHINGTON, DC 20301
ATTN J-3

PROJECT MANAGER
ARMY TACTICAL DATA SYSTEMS
US ARMY ELECTRONICS COMMAND
FORT MONMOUTH, NJ 07703
ATTN DRCPM-TDS-BSI

DIRECTOR
BMD ADVANCED TECH CTR
HUNTSVILLE OFFICE
PO BOX 1500
HUNTSVILLE, AL 35807
ATTN ATC-T

COMMANDER
BMD SYSTEM COMMAND
P.O. BOX 1500
HUNTSVILLE, AL 35807
ATTN BMDSC-AOLIB

COMMANDER
US ARMY ARMOR CENTER
FORT KNOX, KY 40121
ATTN TECHNICAL LIBRARY

DIRECTOR
US ARMY BALLISTIC RESEARCH LABS
ABERDEEN PROVING GROUND, MD 21005
ATTN DRSTE-EL
ATTN DRXBR-AM, W. R. VANANTWERP
ATTN DRDAR-BLE

COMMANDER
US ARMY COMM-ELEC ENGRG INSTAL AGY
FT HUACHUCA, AZ 85613
ATTN CCC-PRSO-S
ATTN CCC-CED-SES

COMMANDER
US ARMY COMMUNICATIONS COMMAND
FORT HUACHUCA, AZ 85613
ATTN CC-ENGR

COMMANDER
US ARMY COMMUNICATIONS COMMAND
COMBAT DEVELOPMENT DIVISION
FT. HUACHUCA, AZ 85613
ATTN ATSI-CD-MD

CHIEF
US ARMY COMMUNICATIONS SYSTEMS AGENCY
FORT MONMOUTH, NJ 07703
ATTN CCM-RD-T, CCM-AD-SV

COMMANDER
US ARMY COMMUNICATIONS & ELECTRONICS
MATERIEL READINESS COMMAND
FORT MONMOUTH, NJ 07703
ATTN DRSEL-CT-HDK, ABRAHAM E. COHEN
ATTN DRSEL-TL-MD, GERHART K. GAULE
ATTN DRSEL-TL-ME
ATTN DRSEL-NL-RO, R. BROWN

COMMANDER
ERADCOM TECHNICAL SUPPORT ACTIVITY
TECHNICAL LIBRARY DIVISION
FORT MONMOUTH, NJ 07703
ATTN DELSD-L

DIRECTOR
US ARMY SIGNALS WARFARE LABORATORY
VINT HILL FARMS STATION
WARRANTON, VA 22186
ATTN DELSW-OS

COMMANDER
US ARMY ELECTRONICS PROVING GROUND
FORT HUACHUCA, AZ 85613
ATTN STEEP-MT-M, GERALD W. DURBIN

DIVISION ENGINEER
US ARMY ENGINEER DIV HUNTSVILLE
P.O. BOX 1600, WEST STATION
HUNTSVILLE, AL 35807
ATTN HNDED-SR

COMMANDER
US ARMY MISSILE RES & DEV COMMAND
REDSTONE ARSENAL, AL 35809
ATTN DRDMI-EAA
ATTN DRDMI-TBD
ATTN DRCPM-PE-EA,
WALLACE O. WAGNER
ATTN DRCPM-PE-EG,
WILLIAM B. JOHNSON

COMMANDER
US ARMY MISSILE MATERIEL
READINESS COMMAND
REDSTONE ARSENAL, AL 35809
ATTN DRCPM-LCEX,
HOWARD H. HENRIKSEN
ATTN DRSMI-TRA,
FAISON P. GIBSON

COMMANDER
US ARMY TANK AUTOMOTIVE COMMAND
WARREN, MI 48090
ATTN DRCPM-GCM-SW, LYLE A. WOLCOTT

COMMANDER
US ARMY TEST AND EVALUATION COMMAND
ABERDEEN PROVING GROUND, MD 21005
ATTN DRSTE-FA

COMMANDER
US ARMY TRAINING AND
DOCTRINE COMMAND
FORT MONROE, VA 23651
ATTN ATORI-OP-SW

PROJECT OFFICER
ARMY TACTICAL COMMUNICATIONS
SYSTEMS
FT MONMOUTH, NJ 07703

COMMANDER
WHITE SANDS MISSILE RANGE
WHITE SANDS MISSILE RANGE,
NM 88002
ATTN TE-AN, MR. OKUMA

CHIEF OF NAVAL RESEARCH
DEPARTMENT OF THE NAVY
ARLINGTON, VA 22217
ATTN CODE 464, R. GRACEN JOINER
ATTN CODE 427

OFFICER-IN-CHARGE
CIVIL ENGINEERING LABORATORY
NAVAL CONSTRUCTION
BATTALION CENTER
PORT HUENEME, CA 93041
ATTN TECHNICAL LIBRARY

COMMANDER
NAVAL AIR SYSTEMS COMMAND
HEADQUARTERS
WASHINGTON, DC 20360
ATTN AIR-350F

COMMANDER
NAVAL ELECTRONIC SYSTEMS COMMAND
HEADQUARTERS
WASHINGTON, DC 20360
ATTN PME-117-215

COMMANDER
NAVAL OCEAN SYSTEMS CENTER
SAN DIEGO, CA 92152
ATTN CODE 812, S. W. LICHTMAN
ATTN CODE 015, C. FLETCHER
ATTN RESEARCH LIBRARY

SUPERINTENDENT (CODE 1424)
NAVAL POSTGRADUATE SCHOOL
MONTEREY, CA 93940
ATTN CODE 1424

COMMANDING OFFICER
NAVAL ORDNANCE STATION
INDIAN HEAD, MD 20640
ATTN STANDARDIZATION DEPT

DIRECTOR
NAVAL RESEARCH LABORATORY
WASHINGTON, DC 20375
ATTN CODE 4104, EMANUAL L. BRANCATO
ATTN CODE 2627, DORIS R. FOLEN
ATTN CODE 7701, JACK D. BROWN
ATTN CODE 7750
ATTN CODE 6624
ATTN CODE 6623, RICHARD L. STATLER

COMMANDER
NAVAL SHIP ENGINEERING CENTER
DEPARTMENT OF THE NAVY
WASHINGTON, DC 20362
(HYATTSVILLE)
ATTN CODE 6174D2, EDWARD F. DUFFY

COMMANDER
NAVAL SURFACE WEAPONS CENTER
WHITE OAK, SILVER SPRING, MD 20910
ATTN CODE 431, EDWIN R. RATHBURN
ATTN L. LIBELLO, CODE WR43
ATTN CODE WA51RH, RM 130-108

COMMANDER
NAVAL WEAPONS CENTER
CHINA LAKE, CA 93555
ATTN CODE 533, TECH LIB

DIRECTOR
STRATEGIC SYSTEMS PROJECT OFFICE
NAVY DEPARTMENT
WASHINGTON, DC 20376
ATTN NSP-2431, GERALD W. HOSKINS
ATTN NSP-230, DAVID GOLD
ATTN NSP-43, TECH LIB
ATTN NSP-27334
ATTN SP 2701, JOHN W. PITSENBERGER
ATTN NSP-2342, RICHARD L. COLENAN

COMMANDER
US NAVAL COASTAL SYSTEMS LABORATORY
PANAMA CITY, FL 32401
ATTN TECH LIB

COMMANDER
ADC/DE
ENT AFB, CO 80912
ATTN DEEDS, JOSEPH C. BRANNAN

AF WEAPONS LABORATORY, AFSC
KIRTLAND AFB, NM 87117
ATTN NT, CARL E. BAUM
ATTN SUL
ATTN ELA, J. P. CASTILLO
ATTN NTS
ATTN SAB
ATTN ELXT
ATTN NT
ATTN CA
ATTN NTN
ATTN ELP

AFTAC
PATRICK AFB, FL 32925
ATTN TFS, MAJ MARION F. SCHNEIDER
ATTN TFE

COMMANDER
AIR UNIVERSITY
MAXWELL AFB, AL 36112
ATTN AUL/LSE-70-250

COMMANDER
ASD
WPAFB, OH 45433
ATTN ENFTV

HEADQUARTERS
ELECTRONIC SYSTEMS DIVISION/YS
HANSCOM AFB, MA 01731
ATTN YSEV

COMMANDER
FOREIGN TECHNOLOGY DIVISION, AFSC
WRIGHT-PATTERSON AFB, OH 45433
ATTN NICD LIBRARY
ATTN ETD, B. L. BALLARD

COMMANDER
OGDEN AIR LOGISTICS CENTER
HILL AFB, UT 84401
ATTN OO-ALC/MMETH, P. W. BERTHEL
ATTN MAJ RONALD BLACKBURN
ATTN MMEDO, LEO KIDMAN

COMMANDER
SACRAMENTO AIR LOGISTICS CENTER
MCCLELLAN AFB, CA 95652
ATTN MMSREM, F. R. SPEAR
ATTN MMARA, J. D. DUGAN
ATTN MMEAE, C. E. HOWARD
ATTN MMCRS, H. A. PELMASTRO
ATTN MMIRA, J. W. DEMES

SAMSO/IN
POST OFFICE BOX 92960
WORLDWAY POSTAL CENTER
LOS ANGELES, CA 90009
(INTELLIGENCE)
ATTN IND, I. J. JUDY

SAMSO/MN
NORTON AFB, CA 92409
(MINUTEMAN)
ATTN MNNH, MAJ M. BARAN
ATTN MNNH, CAPT R. I. LAWRENCE

SAMSO/SK
POST OFFICE BOX 92960
WORLDWAY POSTAL CENTER
LOS ANGELES, CA 90009
(SPACE COMM SYSTEMS)
ATTN SKF

SAMSO/YA
POST OFFICE BOX 92960
WORLDWAY POSTAL CENTER
LOS ANGELES, CA 90009
ATTN YAPC

COMMANDER IN CHIEF
STRATEGIC AIR COMMAND
OFFUTT AFB, NB 68113
ATTN NRI-STINFO LIBRARY
ATTN XPFS, MAJ BRIAN STEPHAN
ATTN DEL
ATTN JPST
ATTN JLTW
ATTN GARNET E. MATZKE

UNIVERSITY OF CALIFORNIA
LAWRENCE LIVERMORE LABORATORY
P.O. BOX 808
LIVERMORE, CA 94550
ATTN TERRY R. DONICH, L-96
ATTN HANS KRUGER, L-96
ATTN LIBRARIAN
ATTN WILLIAM J. HOGAN, L-389
ATTN DONALD J. MEEKER, L-545

LOS ALAMOS SCIENTIFIC LABORATORY
P.O. BOX 1663
LOS ALAMOS, NM 87545
ATTN DOC CON FOR CLARENCE BENTON
ATTN DOC CON FOR JOHN S. MALIK

SANDIA LABORATORIES
PO BOX 5800
ALBUQUERQUE, NM 87115
ATTN DOC CON FOR ORD 9353,
R. L. PARKER
ATTN DOC CON FOR ELMER F. HARTMAN
ATTN C. N. VITTITOE, 5231

US ENERGY RSCH & DEV ADMIN
ALBUQUERQUE OPERATIONS OFFICE
P.O. BOX 5400
ALBUQUERQUE, NM 87115
ATTN OPERATIONAL SAFETY DIV
ATTN DOC CON FOR TECH LIBRARY

CENTRAL INTELLIGENCE AGENCY
ATTN: RD/SI, RM 5G48 HQ BLDG
WASHINGTON, DC 20505
ATTN OSI/NED/NWB

ADMINISTRATOR
DEFENSE ELECTRIC POWER ADMIN
DEPARTMENT OF THE INTERIOR
INTERIOR SOUTH BLDG, 312
WASHINGTON, DC 20240
ATTN L. O'NEILL

DEPARTMENT OF TRANSPORTATION
FEDERAL AVIATION ADMINISTRATION
HEADQUARTERS SEC DIV, ASE-300
800 INDEPENDENCE AVENUE, SW
WASHINGTON, DC 20591
ATTN SEC DIV ASE-300

NATIONAL OCEANIC & ATMOSPHERIC ADMIN
ENVIRONMENTAL RESEARCH LABORATORIES
DEPARTMENT OF COMMERCE
BOULDER, CO 80302
ATTN GLENN JEAN

AEROSPACE CORPORATION
PO BOX 92957
LOS ANGELES, CA 90009
ATTN C. B. PEARLSTON
ATTN IRVING M. GARFUNKEL
ATTN JULIAN REINHEIMER
ATTN LIBRARY
ATTN CHARLES GREENHOW

AGBABIAN ASSOCIATES
250 NORTH NASH STREET
EL SEGUNDO, CA 90245
ATTN LIBRARY

AVCO RESEARCH & SYSTEMS GROUP
201 LOWELL STREET
WILMINGTON, MA 01887
ATTN W. LEPSEVICH

BATTELLE MEMORIAL INSTITUTE
505 KING AVENUE
COLUMBUS, OH 43201
ATTN ROBERT M. BLAZEK
ATTN EUGENE R. LEACH

BDM CORPORATION, THE
7915 JONES BRANCH DRIVE
MCLEAN, VA 22101
ATTN TECHNICAL LIBRARY

BDM CORPORATION, THE
P.O. BOX 9274
ALBUQUERQUE INTERNATIONAL
ALBUQUERQUE, NM 87119
ATTN TECH LIB

BENDIX CORPORATION, THE
NAVIGATION AND CONTROL GROUP
TETERBORO, NJ 07608
ATTN DEPT 6401

BOEING COMPANY, THE
P.O. BOX 3707
SEATTLE, WA 98124
ATTN D. E. ISBELL
ATTN HOWARD W. WICKLEIN, MS 17-11
ATTN DAVID KEMLE
ATTN KENT TECH LIB
ATTN B. C. HANRAHAN

BOOZ-ALLEN AND HAMILTON, INC.
106 APPLE STREET
TINTON FALLS, NJ 07724
ATTN RAYMOND J. CHRISNER
ATTN TECH LIB

BURROUGHS CORPORATION
FEDERAL AND SPECIAL SYSTEMS GROUP
CENTRAL AVE AND ROUTE 252
P.O. BOX 517
PAOLI, PA 19301
ATTN ANGELO J. MAURIELLO

CALSPAN CORPORATION
P.O. BOX 235
BUFFALO, NY 14221
ATTN TECHNICAL LIBRARY

CHARLES STARK DRAPER LABORATORY INC
555 TECHNOLOGY SQUARE
CAMBRIDGE, MA 02139
ATTN TIC, MS 74
ATTN KENNETH FERTIG

CINCINNATI ELECTRONICS CORPORATION
2630 GLENDALE - MILFORD ROAD
CINCINNATI, OH 45241
ATTN LOIS HAMMOND

COMPUTER SCIENCES CORPORATION
P.O. BOX 530
6565 ARLINGTON BLVD
FALLS CHURCH, VA 22046
ATTN RAMONA BRIGGS

COMPUTER SCIENCES CORPORATION
201 LA VETA DRIVE, NE
ALBUQUERQUE, NM 87108
ATTN ALVIN SCHIFF

CONTROL DATA CORPORATION
P.O. BOX 0
MINNEAPOLIS, MN 55440
ATTN JACK MEEHAN

CUTLER-HAMMER, INC.
AIL DIVISION
COMAC ROAD
DEER PARK, NY 11729
ATTN EDWARD KARPEN

DIKEWOOD INDUSTRIES, INC
1009 BRADBURY DRIVE, SE
ALBUQUERQUE, NM 87106
ATTN TECH LIB
ATTN L. WAYNE DAVIS

E-SYSTEMS, INC.
GREENVILLE DIVISION
P.O. BOX 1056
GREENVILLE, TX 75401
ATTN JOLETA MOORE

EFFECTS TECHNOLOGY, INC.
5383 HOLLISTER AVENUE
SANTA BARBARA, CA 93111
ATTN S. CLOW

EG&G, INC.
ALBUQUERQUE DIVISION
PO BOX 10218
ALBUQUERQUE, NM 87114
ATTN C. GILES

FAIRCHILD CAMERA AND INSTRUMENT CORP
464 ELLIS STREET
MOUNTAIN VIEW, CA 94040
ATTN SEC DEPT FOR 2-233,
DAVID K. MYERS

FORD AEROSPACE & COMMUNICATIONS CORP
3939 FABIAN WAY
PALO ALTO, CA 94303
ATTN LIBRARY
ATTN J. T. MATTINGLEY, MS X22
ATTN DONALD R. MCMORROW MS G30

FORD AEROSPACE & COMMUNICATIONS
OPERATIONS
FORD & JAMBOREE ROADS
NEWPORT BEACH, CA 92663
ATTN KEN C. ATTINGER
ATTN E. R. PONCELET, JR.

FRANKLIN INSTITUTE, THE
20TH STREET AND PARKWAY
PHILADELPHIA, PA 19103
ATTN RAMIE H. THOMPSON

GENERAL DYNAMICS CORP
CONVAIR DIVISION
P.O. BOX 80847
SAN DIEGO, CA 92138
ATTN RSCH LIB

GENERAL DYNAMICS CORP
ELECTRONICS DIVISION
P.O. BOX 81127
SAN DIEGO, CA 92138
ATTN RSCH LIB

GENERAL ELECTRIC COMPANY
ORDNANCE SYSTEMS
100 PLASTICS AVENUE
PITTSFIELD, MA 01201
ATTN JOSEPH J. REIDL

GENERAL ELECTRIC COMPANY
TEMPO-CENTER FOR ADVANCED STUDIES
816 STATE STREET (PO DRAWER QQ)
SANTA BARBARA, CA 93102
ATTN DASIAC
ATTN ROYDEN R. RUTHERFORD
ATTN WILLIAM MCNAMERA

GENERAL ELECTRIC COMPANY
AEROSPACE ELECTRONICS SYSTEMS
FRENCH ROAD
UTICA, NY 13503
ATTN CHARLES M. HEWISON, DROP 624

GENERAL ELECTRIC COMPANY-TEMPO
ATTN: DASIAC
C/O DEFENSE NUCLEAR AGENCY
WASHINGTON, DC 20305
ATTN WILLIAM ALFONTE
ATTN ED ARNOLD

GENERAL RESEARCH CORPORATION
P.O. BOX 3587
SANTA BARBARA, CA 93105
ATTN TECH INFO OFFICE

GEORGIA INSTITUTE OF TECHNOLOGY
GEORGIA TECH RESEARCH INSTITUTE
ATLANTA, GA 30332
ATTN R. CURRY

GEORGIA INSTITUTE OF TECHNOLOGY
OFFICE OF CONTRACT ADMINISTRATION
ATTN: RSCH SECURITY COORDINATOR
ATLANTA, GA 30332
ATTN RES & SEC COORD
FOR HUGH DENNY

GRUMMAN AEROSPACE CORPORATION
SOUTH OYSTER BAY ROAD
BETHPAGE, NY 11714
ATTN L-01 35

GTE SYLVANIA, INC.
ELECTRONICS SYSTEMS GRP-EASTERN DIV
77 A STREET
NEEDHAM, MA 02194
ATTN CHARLES A. THORNHILL,
LIBRARIAN
ATTN LEONARD L. BLAISDELL

GTE SYLVANIA, INC.
189 B STREET
NEEDHAM HEIGHTS, MA 02194
ATTN CHARLES H. RAMSBOTTOM
ATTN DAVID P. FLOOD
ATTN COMM SYST DIV, EMIL P. MOTCHOK
ATTN H & V GROUP, MARIO A. NUREFORA
ATTN J. A. WALDRON

HARRIS CORPORATION
HARRIS SEMICONDUCTOR DIVISION
P.O. BOX 883
MELBOURNE, FL 32901
ATTN V. PRES & MGR PRGMS DIV

HONEYWELL INCORPORATED
AVIONICS DIVISION
2600 TIDGEWAY PARKWAY
MINNEAPOLIS, MN 55413
ATTN RONALD R. JOHNSON, A1622
ATTN S&RC LIB

HONEYWELL INCORPORATED
AVIONICS DIVISION
13350 US HIGHWAY 19 NORTH
ST. PETERSBURG, FL 33733
ATTN W. E. STEWART
ATTN M.S. 725-5, STACEY H. GRAFF

HUGHES AIRCRAFT COMPANY
CENTINELLA AND TEALE
CULVER CITY, CA 90230
ATTN CTOC 6/E110
ATTN JOHN B. SINGLETARY, MS 6-D133

IIT RESEARCH INSTITUTE
ELECTROMAG COMPATABILITY ANAL CTR
NORTH SEVERN
ANNAPOLIS, MD 21402
ATTN ACOAT

IIT RESEARCH INSTITUTE
10 WEST 35TH STREET
CHICAGO, IL 60616
ATTN IRVING N. MINDEL
ATTN JACK E. BRIDGES

INSTITUTE FOR DEFENSE ANALYSES
400 ARMY-NAVY DRIVE
ARLINGTON, VA 22202
ATTN TECH INFO OFC

INTL TEL & TELEGRAPH CORPORATION
500 WASHINGTON AVENUE
NUTLEY, NJ 07110
ATTN TECHNICAL LIBRARY

ION PHYSICS CORPORATION
SOUTH BEDFORD STREET
BURLINGTON, MA 01803
ATTN ROBERT D. EVANS

IRT CORPORATION
P.O. BOX 81087
SAN DIEGO, CA 92138
ATTN DENNIS SWIFT
ATTN C. B. WILLIAMS

JAYCOR
1401 CAMINO DEL MAR
DEL MAR, CA 92014
ATTN ERIC P. WENAAS
ATTN RALPH H. STAHL

JAYCOR
205 S WHITTING STREET, SUITE 500
ALEXANDRIA, VA 22304
ATTN TECH LIB

KAMAN SCIENCES CORPORATION
P.O. BOX 7463
COLORADO SPRINGS, CO 80933
ATTN ALBERT P. BRIDGES
ATTN W. FOSTER RICH
ATTN WALTER E. WARE
ATTN JERRY I. LUBELL
ATTN JOHN R. HOFFMAN
ATTN FRANK H. SHELTON

LITTON SYSTEMS, INC.
DATA SYSTEMS DIVISION
8000 WOODLEY AVENUE
VAN NUYS, CA 91409
ATTN M848-61
ATTN EMC GP

LITTON SYSTEMS, INC.
GUIDANCE & CONTROL SYSTEMS DIVISION
5500 CANOGA AVENUE
WOODLAND HILLS, CA 91364
ATTN JOE MOYER

LITTON SYSTEMS, INC.
AMECOM DIVISION
5115 CALVERT ROAD
COLLEGE PARK, MD 20740
ATTN J. SKAGGS

LOCKHEED MISSILES AND
SPACE COMPANY, INC.
P.O. BOX 504
SUNNYVALE, CA 94088
ATTN DEPT 85-85, SAMUEL I. TAIMUTY
ATTN G. F. HEATH, D/81-14
ATTN EDWIN A. SMITH, DEPT 85-85
ATTN H. E. THAYN
ATTN L. ROSSI, DEPT 81-64
ATTN BENJAMIN T. KIMURA, DEPT 81-14

LOCKHEED MISSILES AND SPACE CO INC
3251 HANOVER STREET
PALO ALTO, CA 94304
ATTN TECH INFO CTR, D/COLL

M.I.T. LINCOLN LABORATORY
P.O. BOX 73
LEXINGTON, MA 02173
ATTN LEONA LOUGHLIN,
LIBRARIAN A-082

MARTIN MARIETTA AEROSPACE
ORLANDO DIVISION
P.O. BOX 5837
ORLANDO, FL 32805
ATTN MONA C. GRIFFITH, LIB MP-30

EXXON NUCLEAR COMPANY, INC
RESEARCH & TECHNOLOGY CENTER
2955 GEORGE WASHINGTON WAY
RICHLAND, WA 99352
ATTN DR. A. W. TRIVELPIECE

MCDONNELL DOUGLAS CORPORATION
POST OFFICE BOX 516
ST. LOUIS, MO 63166
ATTN TOM ENDER

MCDONNELL DOUGLAS CORPORATION
5301 BOLSA AVENUE
HUNTINGTON BEACH, CA 92647
ATTN STANLEY SCHNEIDER
ATTN TECH LIBRARY SERVICES

MISSION RESEARCH CORPORATION
735 STATE STREET
SANTA BARBARA, CA 93101
ATTN WILLIAM C. HART
ATTN EMP GROUP

MISSION RESEARCH CORPORATION
P.O. BOX 8693, STATION C
ALBUQUERQUE, NM 87108
ATTN DAVID E. MEREWETHER
ATTN L. N. MCCORMICK

MISSION RESEARCH CORPORATION-
SAN DIEGO
P.O. BOX 1209
LA JOLLA, CA 92038
ATTN V. A. J. VAN LINT

MITRE CORPORATION, THE
P.O. BOX 208
BEDFORD, MA 01730
ATTN THEODORE JARVIS
ATTN M. E. FITZGERALD

NORTHROP RESEARCH TECHNOLOGY CENTER
ONE RESEARCH PARK
PALOS VERDES PENN, CA 90274
ATTN LIBRARY

NORTHROP CORPORATION
ELECTRONIC DIVISION
2301 WEST 120TH STREET
HAWTHORNE, CA 90250
ATTN VINCENT R. DEMARTINO
ATTN TECH LIB
ATTN LEW SMITH
ATTN RAD EFFECTS GRP, B. AHLPORT

PHYSICS INTERNATIONAL COMPANY
2700 MERCED STREET
SAN LEANDRO, CA 94577
ATTN DOC CON

PULSAR ASSOCIATES, INC.
7911 HERSCHEL AVENUE
LA JOLLA, CA 92037
ATTN V. FARGO
ATTN SECURITY

R & D ASSOCIATES
PO BOX 9695
MARINA DEL REY, CA 90291
ATTN S. CLAY ROGERS
ATTN LEONARD SCHLESSINGER
ATTN CHARLES MO
ATTN RICHARD R. SCHAEFER
ATTN DOC CON

RAND CORPORATION, THE
1700 MAIN STREET
SANTA MONICA, CA 90406
ATTN LIB-D
ATTN CULLEN CRAIN

RAY PROOF CORPORATION
P.O. BOX 60
NORWICK, CT 06856
ATTN E. S. KESNER

RAYTHEON COMPANY
HARTWELL ROAD
BEDFORD, MA 01730
ATTN GAJANAN H. JOSHI,
RADAR SYS LAB

RAYTHEON COMPANY
528 BOSTON POST ROAD
SUDBURY, MA 01776
ATTN HAROLD L. FLESCHER

RCA CORPORATION
CAMDEN COMPLEX
FRONT & COOPER STREETS
CAMDEN, NJ 08012
ATTN R. W. ROSTROM, 13-5-2
ATTN OLIVE WHITEHEAD

ROCKWELL INTERNATIONAL CORPORATION
P.O. BOX 3105
ANAHEIM, CA 92803
ATTN J. L. MONROE, DEPT 243-027,
DIV 031
ATTN D/243-068, 031-CA31
ATTN V. J. MICHEL

ROCKWELL INTERNATIONAL CORPORATION
SPACE DIVISION
12214 SOUTH LAKEWOOD BOULEVARD
DOWNEY, CA 90241
ATTN B. E. WHITE

ROCKWELL INTERNATIONAL CORPORATION
5701 WEST IMPERIAL HIGHWAY
LOS ANGELES, CA 90009
ATTN B-1 DIV TIC (BA08)

SCIENCE APPLICATIONS, INC.
P.O. BOX 277
BERKELEY, CA 94701
ATTN FREDERICK M. TESCHE

SCIENCE APPLICATIONS, INC.
PO BOX 2351
LA JOLLA, CA 92038
ATTN R. PARKINSON

SCIENCE APPLICATIONS, INC.
HUNTSVILLE DIVISION
2109 W. CLINTON AVENUE
SUITE 700
HUNTSVILLE, AL 35805
ATTN NOEL R. BYRN

SCIENCE APPLICATIONS, INC.
8400 WESTPARK DRIVE
MCLEAN, VA 22101
ATTN WILLIAM L. CHADSEY

SINGER COMPANY, THE
ATTN: SECURITY MANAGER
1150 MC BRIDE AVENUE
LITTLE FALLS, NJ 07424
ATTN TECH INFO CTR

SPERRY FLIGHT SYSTEMS DIVISION
SPERRY RAND CORPORATION
P.O. BOX 21111
PHOENIX, AZ 85036
ATTN D. ANDREW SCHOW

SPERRY RAND CORPORATION
SPERRY MICROWAVE ELECTRONICS
P.O. BOX 4648
CLEARWATER, FL 33518
ATTN MARGARET CORT

SPERRY RAND CORPORATION
SPERRY DIVISION
MARCUS AVENUE
GREAT NECK, NY 11020
ATTN TECH LIB

SPIRE CORPORATION
P.O. BOX D
PATRIOTS PARK
BEDFORD, MA 01730
ATTN ROGER G. LITTLE

SRI INTERNATIONAL
333 RAVENSWOOD AVENUE
MENLO PARK, CA 94025
ATTN GEORGE CARPENTER
ATTN ARTHUR LEE WHITSON

SRI INTERNATIONAL
306 WYNN DRIVE, N. W.
HUNTSVILLE, AL 35805
ATTN MR. HULLINGS

DISTRIBUTION (Cont'd)

SYSTEMS, SCIENCE AND SOFTWARE, INC.
PO BOX 1620
LA JOLLA, CA 92038
ATTN ANDREW R. WILSON

TEXAS INSTRUMENTS, INC.
P.O. BOX 6015
DALLAS, TX 75222
ATTN TECH LIB
ATTN DONALD J. MANUS, MS 72

TEXAS TECH UNIVERSITY
P.O. BOX 5404 NORTH COLLEGE STATION
LUBBOCK, TX 79417
ATTN TRAVIS L. SIMPSON

TRW DEFENSE & SPACE SYS GROUP
ONE SPACE PARK
REDONDO BEACH, CA 90278
ATTN O. E. ADAMS, R1-1144
ATTN ROBERT M. WEBB, R1-2410
ATTN R. K. PLEBUCH, R1-2078
ATTN H. H. HOLLOWAY, R1-2036
ATTN L. R. MAGNOLIA

TRW SYSTEMS GROUP
P.O. BOX 368
CLEARFIELD, UT 84015
ATTN DONALD W. PUGSLEY

UNITED TECHNOLOGIES CORP
NORDEN DIVISION
HELEN STREET
NORWALK, CT 06851
ATTN TECH LIB

UNITED TECHNOLOGIES CORPORATION
HAMILTON STANDARD DIVISION
BRADLEY INTERNATIONAL AIRPORT
WINDSOR LOCKS, CT 06069
ATTN CHIEF ELEC DESIGN

VECTOR RESEARCH ASSOCIATES
735 STATE STREET
SANTA BARBARA, CA 93101
ATTN W. A. RADASKY

WESTINGHOUSE ELECTRIC CORPORATION
ADVANCED ENERGY SYSTEMS DIV
P.O. BOX 10864
PITTSBURGH, PA 15236
ATTN TECH LIB

US ARMY ELECTRONICS RESEARCH
& DEVELOPMENT COMMAND
ATTN WISEMAN, ROBERT S., DR., DRDEL-CT

HARRY DIAMOND LABORATORIES
ATTN 00100, COMMANDER/TECH DIR/TSO
ATTN CHIEF, DIV 10000
ATTN CHIEF, DIV 20000
ATTN CHIEF, DIV 30000
ATTN CHIEF, DIV 40000
ATTN RECORD COPY, 81200
ATTN HDL LIBRARY, (3 COPIES) 81100
ATTN HDL LIBRARY, (WOODBRIDGE) 81100
ATTN TECHNICAL REPORTS BRANCH, 81300
ATTN CHAIRMAN, EDITORIAL COMMITTEE
ATTN CHIEF, 21000
ATTN CHIEF, 21100
ATTN CHIEF, 21200
ATTN CHIEF, 21300 (20 COPIES)
ATTN CHIEF, 21400
ATTN CHIEF, 21500
ATTN CHIEF, 22000
ATTN CHIEF, 22100
ATTN CHIEF, 22300
ATTN CHIEF, 22800
ATTN CHIEF, 22900
ATTN CHIEF, 20240